The Osmium(VIII) Oxofluoro Cations $OsO_2F_3^+$ and $F(cis\text{-}OsO_2F_3)_2^+$: Syntheses, Characterization by ^{19}F NMR Spectroscopy and Raman Spectroscopy, X-ray Crystal Structure of $F(cis\text{-}OsO_2F_3)_2^+Sb_2F_{11}^-$, and Density Functional Theory Calculations of $OsO_2F_3^+$, ReO_2F_3, and $F(cis\text{-}OsO_2F_3)_2^+$ †

William J. Casteel, Jr.,[1] David A. Dixon,[2] Hélène P. A. Mercier,[1] and Gary J. Schrobilgen*,[1]

Department of Chemistry McMaster University, Hamilton, Ontario L8S 4M1, Canada, and Environmental Molecular Sciences Laboratory, Pacific Northwest National Laboratory, Battelle Memorial Insitute P.O. Box 999, KI-83, Richland, Washington 99352

Received August 10, 1995[⊗]

Osmium dioxide tetrafluoride, *cis*-OsO_2F_4, reacts with the strong fluoride ion acceptors AsF_5 and SbF_5 in anhydrous HF and SbF_5 solutions to form orange salts. Raman spectra are consistent with the formation of the fluorine-bridged diosmium cation $F(cis\text{-}OsO_2F_3)_2^+$, as the AsF_6^- and $Sb_2F_{11}^-$ salts, respectively. The ^{19}F NMR spectra of the salts in HF solution are exchange-averaged singlets occurring at higher frequency than those of the fluorine environments of *cis*-OsO_2F_4. The $F(cis\text{-}OsO_2F_3)_2^+Sb_2F_{11}^-$ salt crystallizes in the orthorhombic space group *Imma*. At −107 °C, $a = 12.838(3)$ Å, $b = 10.667(2)$ Å, $c = 11.323(2)$ Å, $V = 1550.7(8)$ Å^3, and $Z = 4$. Refinement converged with $R = 0.0469$ [$R_w = 0.0500$]. The crystal structure consists of discrete fluorine-bridged $F(cis\text{-}OsO_2F_3)_2^+$ and $Sb_2F_{11}^-$ ions in which the fluorine bridge of the $F(cis\text{-}OsO_2F_3)_2^+$ cation is *trans* to an oxygen atom (Os−O 1.676 Å) of each OsO_2F_3 group. The angle at the bridge is 155.2(8)° with a bridging Os---F_b distance of 2.086(3) Å. Two terminal fluorine atoms (Os−F 1.821 Å) are *cis* to the two oxygen atoms (Os−O 1.750 Å), and two terminal fluorine atoms of the OsO_2F_3 group are *trans* to one another (1.813 Å). The $OsO_2F_3^+$ cation was characterized by ^{19}F NMR and by Raman spectroscopy in neat SbF_5 solution but was not isolable in the solid state. The NMR and Raman spectroscopic findings are consistent with a trigonal bipyramidal cation in which the oxygen atoms and a fluorine atom occupy the equatorial plane and two fluorine atoms are in axial positions. Density functional theory calculations show that the crystallographic structure of $F(cis\text{-}OsO_2F_3)_2^+$ is the energy-minimized structure and the energy-minimized structures of the $OsO_2F_3^+$ cation and ReO_2F_3 are trigonal bipyramidal having C_{2v} point symmetry. Attempts to prepare the $OsOF_5^+$ cation by oxidative fluorination of *cis*-OsO_2F_4 with $KrF^+AsF_6^-$ in anhydrous HF proved unsuccessful.

Introduction

The fluoride ion donor properties of a considerable number of oxide fluorides of the main-group elements toward strong fluoride ion acceptors have been studied by X-ray diffraction, vibrational spectroscopy, and NMR spectroscopy. The adducts are essentially ionic in nature and consist of discrete cations that are weakly coordinated to the fluoro anion by means of fluorine bridges and are exemplified by the salts of the fluoro and oxofluoro cations of the noble gases.[3,4] Although SbF_5 is a significantly stronger fluoro acid than the oxide fluorides of the transition metals, adducts with a limited number of d- and f-block metal oxide fluorides have been reported, e.g., $MOF_4 \cdot SbF_5$ (M = Mo, W, Re, U),[5−7] $ReOF_5 \cdot SbF_5$,[8] $UOF_4 \cdot 2BiF_5$,[9] $UOF_4 \cdot nSbF_5$ ($n = 2, 3$),[6,7] $UO_2F_2 \cdot nSbF_5$ ($n = 2-4$),[10,11] and $UOF_4 \cdot nSbF_5 \cdot mCH_3CN$ ($n = 1$ or 2, $m = 2$ or 6).[12] A number of transition metal oxide fluoride adducts with weaker main-group and transition metal pentafluorides have also been investigated, e.g., $ReOF_4 \cdot AsF_5$[8] and $UOF_4 \cdot 3M'F_5$ (M′ = Nb, Ta).[9] Unlike the main-group adducts, the MOF_4 and UO_2F_2 adducts of SbF_5 studied to date by X-ray crystallography[5,7,10] have been shown to be extensively associated by means of M---F---Sb fluorine bridges. Only the $ReOF_5 \cdot SbF_5$ adduct has been shown to contain a discrete oxofluoro cation consisting of Re---F---Re-bridged $F(ReOF_4)_2^+$ cations and $Sb_2F_{11}^-$ anions.[8]

Until recently, the chemistry of osmium in its highest oxidation state, +8, was limited to OsO_4,[13−18] OsO_3F_2 ,[18−27] and their structurally ill-defined fluoro anions $OsO_4F_2^{2-}$ [27] and $OsO_3F_3^-$.[27,28] A new osmium(VIII) oxide fluoride was recently

⊗ Abstract published in *Advance ACS Abstracts,* June 15, 1996.

† Dedicated to Dr. Roland Bougon on the occasion of his 60th birthday.

(1) McMaster University
(2) Pacific Northwest National Laboratory.
(3) (a) Selig, H.; Holloway, J. H. Cationic and Anionic Complexes of the Noble Gases. In *Topics in Current Chemistry*; Boschke, F. L., Ed.; Springer-Verlag: Berlin, 1984; Vol. 124, pp 33−90. (b) Schrobilgen, G. J.; Whalen, J. M. Helium-Group Gases, Compounds. In *Kirk-Othmer Encyclopedia of Chemical Technology*, 4th ed.; Wiley: New York, 1994; Chapter 13, pp 38−53.
(4) Mercier, H. P. A.; Sanders, J. C. P.; Schrobilgen, G. J.; Tsai, S. S *Inorg. Chem.* **1993**, *32*, 386.
(5) Fawcett, J.; Holloway, J. H.; Russell, D. R. *J. Chem. Soc., Dalton Trans.* **1981**, 1212.
(6) Bougon, R.; Fawcett, J.; Holloway, J. H.; Russell, D. R. *C. R. Acad. Sci. Paris* **1978**, *287C*, 423.
(7) Bougon, R.; Fawcett, J.; Holloway, J. H.; Russell, D. R. *J. Chem. Soc., Dalton Trans.* **1979**, 1881.
(8) Schrobilgen, G. J.; Holloway, J. H.; Russell, D. R. *J. Chem. Soc., Dalton Trans.* **1984**, 1411.
(9) Holloway, J. H.; Laycock, D.; Bougon, R. *J. Chem. Soc., Dalton Trans.* **1983**, 2303.
(10) Fawcett, J.; Holloway, J. H.; Laycock, D.; Russell, D. R. *J. Chem. Soc., Dalton Trans.* **1982**, 1355.
(11) Holloway, J. H.; Laycock, D.; Bougon, R. *J. Chem. Soc., Dalton Trans.* **1982**, 1635.
(12) Holloway, J. H.; Laycock, D.; Bougon, R. *J. Fluorine Chem.* **1984**, *26*, 281.
(13) *Gmelin Handbuch der Anorganischen Chemie*, 8th ed.; Springer: Berlin, 1980; Suppl. Vol. 1.
(14) Seip, H. M.; Stølevik, R. *Acta Chem. Scand.* **1966**, *20*, 385.
(15) Almenningen, A.; Bastiansen, O.; Haaland, A; Seip, H. M. *Angew. Chem., Int. Ed. Engl.* **1965**, *4*, 819.
(16) Jezowska-Trzebiatowska, B.; Hanuza, J. *Acta Phys. Pol. A* **1970**, *38*, 563.
(17) Krebs, B.; Hasse, K. *Acta Crystallogr., Sect. B* **1976**, *32*, 1334.
(18) Holloway, J. H.; Laycock, D. *Adv. Inorg. Chem. Radiochem.* **1984**, *28*, 73.
(19) Hepworth, M. A.; Robinson, P. L. *J. Inorg. Nucl. Chem.* **1957**, *4*, 24.

S0020-1669(95)01059-7 CCC: $12.00

obtained from the reaction of KrF_2 and OsO_4 in anhydrous HF solution[29,30] and has been shown by material balance, electron diffraction, ^{19}F NMR spectroscopy, $^{19}F\{^{187}Os\}$ inverse correlation NMR spectroscopy, vibrational spectroscopy, density functional theory calculations,[31] and a disordered X-ray crystal structure[26] to be *cis*-OsO_2F_4. The present study investigates the fluoride ion donor properties of *cis*-OsO_2F_4, the most highly fluorinated oxide fluoride of Os(VIII) presently known, and represents the first report of cationic osmium(VIII) species.

Results and Discussion

Syntheses of the $OsO_2F_3^+$ and $F(cis\text{-}OsO_2F_3)_2^+$ Cations and Solution Characterization by ^{19}F NMR Spectroscopy. Deep-burgundy-colored *cis*-OsO_2F_4 readily dissolves in anhydrous HF solvent in the presence of the strong fluoride ion acceptors SbF_5 and AsF_5 to form orange solutions which are stable at room temperature (eqs 1 and 2). Removal of HF under

$$2\ cis\text{-}OsO_2F_4 + 2SbF_5 \xrightarrow{\text{HF, 25 °C}} F(cis\text{-}OsO_2F_3)_2^+Sb_2F_{11}^- \quad (1)$$

$$2\ cis\text{-}OsO_2F_4 + AsF_5 \xrightarrow{\text{HF, 25 °C}} F(cis\text{-}OsO_2F_3)_2^+AsF_6^- \quad (2)$$

vacuum at −10 °C from samples containing 1:1 molar ratios of *cis*-OsO_2F_4 and SbF_5 and at −78 °C from samples containing a 4-fold excess of AsF_5 yields orange solid adducts according to eqs 1 and 2 which dissociate back to *cis*-OsO_2F_4 and the pentafluorides at room temperature under static vacuum. While the $Sb_2F_{11}^-$ salt was sufficiently stable to allow manipulation of single crystals in a dry nitrogen atmosphere without significant decomposition, the AsF_6^- salt was much less stable, having a dissociation pressure of ca. 150 Torr at 23 °C.

Under dilute conditions (ca. 0.03 M), *cis*-OsO_2F_4 dissolves in neat SbF_5 to give a yellow solution of the $OsO_2F_3^+$ cation according to eq 3. The ^{19}F NMR spectra (Figure 1) of these

$$cis\text{-}OsO_2F_4 + nSbF_5 \rightarrow OsO_2F_3^+Sb_nF_{5n+1}^- \quad (3)$$

solutions at 30 °C comprise a doublet (122.4 ppm) and a triplet (129.5 ppm) having relative intensities of 2:1 [$^2J(^{19}F-^{19}F)$ = 164 Hz; $\Delta\nu_{1/2}$ = 70 Hz] and are consistent with a trigonal bipyramidal $OsO_2F_3^+$ cation in which the oxygen atoms are in equatorial positions. The fluorine resonances are significantly more deshielded than in *cis*-OsO_2F_4 (15.8 and 63.3 ppm),[31] which is in accord with the higher electronegativity anticipated for osmium in the cation. The $Sb_nF_{5n+1}^-/(SbF_5)_n$ resonances occur at −87.2 (1), −105.2 (2), −131.0 (2) ppm (relative intensities in parentheses; $\Delta\nu_{1/2}$ = 1370−1830 Hz) and collapse into a single broad exchange-averaged line (−110 ppm, $\Delta\nu_{1/2}$ = 3140 Hz) at 56 °C accompanied by broadening of the doublet and triplet of the $OsO_2F_3^+$ cation ($\Delta\nu_{1/2} \approx 100$ Hz). Attempts were made to narrow the $OsO_2F_3^+$ cation resonances sufficiently to permit observation of ^{187}Os satellites arising from spin−spin coupling of ^{19}F to ^{187}Os ($I = {}^1/_2$, 1.64% natural abundance; cf. ref 31). Addition of XeF_2 to SbF_5 solutions[32] of $OsO_2F_3^+$ resulted in the anticipated lower solvent viscosity at temperatures as low as 7 °C and in the formation of XeF^+ [−290.1 ppm; $^1J(^{129}Xe-^{19}F)$ = 7194 Hz] and $Sb_nF_{5n+1}^-$ ions [$Sb_nF_{5n+1}^-/(SbF_5)_n$ occur at −87.2 (1), −105.4 (2), −131.0 (3) ppm, $\Delta\nu_{1/2}$ = 1530 Hz]. In view of the small magnitudes of the natural-abundance $^{187}Os-^{19}F$ couplings in *cis*-OsO_2F_4 (35.1 and 59.4 Hz), which are also anticipated to be small in $OsO_2F_3^+$, and the low natural abundance of ^{187}Os, it is clear that the ^{187}Os satellites are masked by the breadths of ^{19}F NMR multiplets. The $OsO_2F_3^+$ cation doublet (130.2 ppm) and triplet (122.4 ppm) line widths at 7 °C ($\Delta\nu_{1/2}$ = 50 Hz) were not narrowed sufficiently to permit the observation of ^{187}Os satellites. In related attempts to produce a lower viscosity solvent medium, HF (0.8 mol %) was added to SbF_5 solutions of the $OsO_2F_3^+$ cation, yielding a single exchange-averaged resonance at 122.18 ppm (30 °C, $\Delta\nu_{1/2}$ = 71 Hz) assigned to F-on-Os(VIII) and an intense broad peak at −117.2 ppm ($\Delta\nu_{1/2}$ = 285 Hz) attributed to exchange-averaged HF and $Sb_nF_{5n+1}^-$. The high-frequency position of the F-on-Os(VIII) resonance is similar to the weighted average for the axial and equatorial fluorine environments of $OsO_2F_3^+$ in pure SbF_5 solvent (124.8 ppm, 30 °C) and is consistent with $OsO_2F_3^+$ as the dominant species. Removal of SbF_5 under vacuum from solutions of $OsO_2F_3^+$ in pure SbF_5 gave deep red-orange solutions just prior to the appearance of an orange solid. The Raman spectrum of the orange solid was identical to that observed for $F(cis\text{-}OsO_2F_3)_2^+Sb_2F_{11}^-$, with the exception of the Sb−F stretching and bending frequencies associated with the polymeric $Sb_nF_{5n+1}^-$ anion and SbF_5 (see **Raman Spectroscopy and Vibrational Assignments**). The solid and liquid mixture was observed at a *cis*-OsO_2F_4:SbF_5 ratio of 1:1.27.

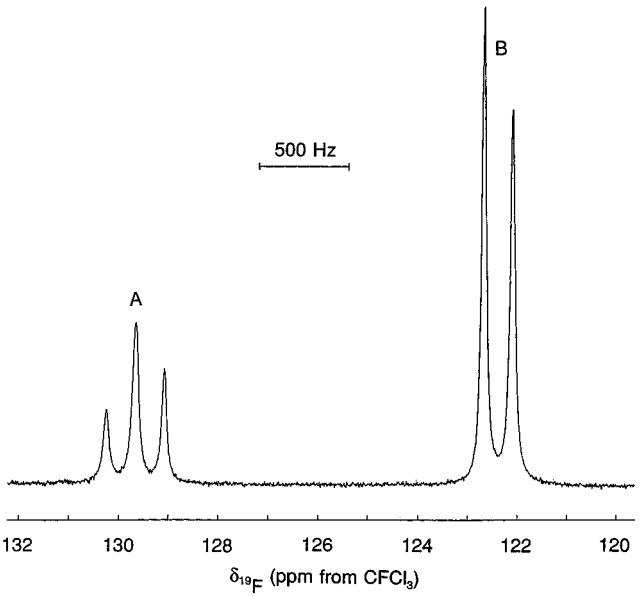

Figure 1. ^{19}F NMR spectrum (282.409 MHz) of the $OsO_2F_3^+$ cation recorded at 7 °C in SbF_5 solvent containing $XeF^+Sb_nF_{5n+1}^-$: (A) equatorial fluorine; (B) axial fluorines.

Fluorine-19 NMR spectra of the AsF_6^- and $Sb_2F_{11}^-$ salts of the $F(cis\text{-}OsO_2F_3)_2^+$ cation were recorded at 30 °C in HF solution; spectra were not recorded at lower temperatures because both salts are essentially insoluble at 0 °C. The

(20) Nguyen-Nghi; Bartlett, N. *C. R. Acad. Sci. Paris, Sect. C* **1969**, *756*, 269.
(21) Beattie, I. R.; Livingston, K. M. S.; Reynolds, D. J.; Ozin, G. A. *J. Chem. Soc. A* **1970**, 1210.
(22) Sunder, W. A.; Stevie, F. A. *J. Fluorine Chem.* **1975**, *6*, 449.
(23) Beattie, I. R. *J. Raman Spectrosc.* **1976**, *4*, 313.
(24) Jones, P. J.; Levason, W.; Tajik, M. *J. Fluorine Chem.* **1984**, *25*, 195.
(25) (a) Hope, E. G.; Levason, W.; Ogden, J. S. *J. Chem. Soc., Dalton Trans.* **1988**, 61. (b) Hope, E. G.; Levason, W.; Ogden, J. S. *J. Chem. Soc., Dalton Trans.* **1988**, 997.
(26) Bougon, R.; Burr, B.; Seppelt, K. *Chem. Ber.* **1993**, *126*, 1331.
(27) Brewer, S. A.; Brisdon, A. K.; Holloway, J. H.; Hope, E. G.; Levason, W.; Ogden, J. S.; Saad, A. K. *J. Fluorine Chem.* **1993**, *60*, 13.
(28) Griffith, W. P. *J. Chem. Soc. A* **1969**, 211.
(29) Bougon, R. *J. Fluorine Chem.* **1991**, *53*, 419.
(30) Christe, K. O.; Bougon, R. *J. Chem. Soc., Chem. Commun.* **1992**, 1056.
(31) Christe, K. O.; Dixon, D. A.; Mack, H. G.; Oberhammer, H.; Pagelot, A.; Sanders, J. C. P.; Schrobilgen, G. J. *J. Am. Chem. Soc.* **1993**, *115*, 11279.
(32) Gillespie, R. J.; Schrobilgen, G. J. *Inorg. Chem.* **1974**, *13*, 2370.

Table 1. Summary of Crystal Data and Refinement Results for $F(cis\text{-}OsO_2F_3)_2^+Sb_2F_{11}^-$

space group	*Imma* (No. 74)
a (Å)	12.838(3)
b (Å)	10.667(2)
c (Å)	11.323(2)
V (Å^3)	1550.7(8)
Z (molecules/unit cell)	4
mol. wt	1029.9
calcd density (g cm^{-3})	4.411
T (°C)	−107
color	orange
μ (cm^{-1})	199.90
wavelength (Å) used for data collcn	0.56086
final agreement factors	$R^a = 0.0469$
	$R_w{}^b = 0.0500$

[a] $R = \sum||F_o| - |F_c||/\sum|F_o|$. [b] $R_w = \sum|(|F_o| - |F_c|)w^{1/2}|/\sum(|F_o|w)$ where $w = 1/[\sigma^2(F) + 0.006029F^2]$.

spectrum of the AsF_6^- salt was recorded in the presence of a 17-fold molar excess of AsF_5 with respect to the $F(cis\text{-}OsO_2F_3)_2^+$ cation. Singlets were observed at 81.0 ($\Delta\nu_{1/2} = 2260$ Hz) and 101.1 ($\Delta\nu_{1/2} = 510$ Hz) ppm, respectively, which are deshielded with respect to *cis*-OsO_2F_4[31] and which are in accord with cation formation. The observation of a single fluorine environment is attributed to rapid fluorine exchange among cation environments and is consistent with equilibria 4−6. The ^{19}F resonances of excess Lewis acid, the anion, and HF solvent

$$F(cis\text{-}OsO_2F_3)_2^+ \rightleftharpoons cis\text{-}OsO_2F_4 + OsO_2F_3^+ \quad (4)$$

$$F(cis\text{-}OsO_2F_3)_2^+ + 2HF \rightleftharpoons 2cis\text{-}OsO_2F_4 + H_2F^+ \quad (5)$$

$$OsO_2F_3^+ + 2HF \rightleftharpoons cis\text{-}OsO_2F_4 + H_2F^+ \quad (6)$$

are also exchange-averaged, giving broad resonances at −170.5 ($\Delta\nu_{1/2} = 425$ Hz) and −135.7 ppm ($\Delta\nu_{1/2} = 387$ Hz) in the $Sb_2F_{11}^-$ and AsF_6^-/AsF_5 cases, respectively. Equilibria 5 and 6 are suppressed in the presence of excess Lewis acid so that the exchange-averaged F-on-Os(VIII) resonance occurs at highest frequency in solutions containing a large excess of AsF_5.

Attempts to prepare the $OsOF_5^+$ cation by fluorination of *cis*-OsO_2F_4 with excess KrF_2 in the presence of excess AsF_5 in HF solvent resulted in the isolation of $F(cis\text{-}OsO_2F_3)_2^+AsF_6^-$ according to eq 7.

$$2cis\text{-}OsO_2F_4 + KrF_2 + AsF_5 \xrightarrow{HF,\ -20\ °C} F(cis\text{-}OsO_2F_3)_2^+AsF_6^- + F_2 + Kr \quad (7)$$

X-ray Crystal Structure of $F(cis\text{-}OsO_2F_3)_2^+Sb_2F_{11}^-$. Details of the data collection parameters and other crystallographic information for $F(cis\text{-}OsO_2F_3)_2^+Sb_2F_{11}^-$ (*Imma* space group) are given in Table 1. The final atomic coordinates and equivalent isotropic thermal parameters are summarized in Table 2. Important bond lengths and angles for $F(cis\text{-}OsO_2F_3)_2^+Sb_2F_{11}^-$ are listed in Table 3. The cation and anion are depicted in Figure 2, and a stereoview of the unit cell is given in the Supporting Information (Figure 4).

The crystal structure of $F(cis\text{-}OsO_2F_3)_2^+Sb_2F_{11}^-$ consists of well-separated $F(cis\text{-}OsO_2F_3)_2^+$ cations and $Sb_2F_{11}^-$ anions. The oxygen and fluorine atoms of the cation were readily assigned on the basis of their bond lengths with osmium. The cation consists of two symmetry-related $[OsO_2F_3]$ units bridged by a fluorine atom *trans* to two Os−O bonds. The coordination sphere of each osmium atom consists of two oxygen atoms and two fluorine atoms that are *cis* to one another and two symmetry-related fluorine atoms that are *trans* to one another, providing a distorted octahedral environment around each osmium atom (Figure 2a) that is similar to the *cis*-dioxo arrangements found in *cis*-OsO_2F_4[31] and in the $[TcO_2F_4]$ units of the infinite-chain polymer, TcO_2F_3.[33] The impeller-shaped ellipsoids of the light atoms of the cation suggested the presence of a positional or static (thermal) disorder.[34,35] Resolution of two positions for the bridging fluorine atom, F(3), demonstrated that the disorder is positional in nature and involves two $F(cis\text{-}OsO_2F_3)_2^+$ cations. A similar positional disorder was observed for the $Sb_2F_{11}^-$ anion, but was better resolved (*vide infra*). Although the disorder on the bridging fluorine atom of $F(cis\text{-}OsO_2F_3)_2^+$ was resolved (the two F(3) atoms are separated by 0.76(3) Å), the disorder on the other light atoms could not be resolved because the two sites were closer than 0.561 Å, the data resolution limit. Because such disorders are accompanied by shortening of the bond lengths, corrections were made for librational motion by performing a standard rigid-body librational analysis. Bond lengths referred to in the subsequent discussion and in Table 3 are the librationally corrected values and are longer than the uncorrected distances. It is noted that the correction for the O(1) atom, which has the largest isotropic thermal ellipsoid, is

Table 2. Atomic Coordinates ($\times 10^4$) and Equivalent Isotropic Displacement Coefficients (Å^2 $\times$ 10^3) for $F(cis\text{-}OsO_2F_3)_2^+Sb_2F_{11}^-$

	x	y	z	$U_{eq}{}^a$	sof[b]
Os(1)	0	590(1)	2264(1)	20(1)	0.5
F(1)	0	1070(10)	748(9)	73(6)	0.5
F(2)	−1356(8)	860(14)	2244(11)	97(5)	1.0
O(1)	0	681(9)	3789(9)	30(2)	0.5
O(2)	0	−943(11)	2054(14)	63(6)	0.5
F(3)	297(12)	2500	2472(15)	28(3)	0.25
Sb(1)	7262(1)	7500	759(1)	26(1)	0.5
F(4)	6616(15)	9023(17)	1018(19)	62(2)	0.5
F(5)	6024(14)	8313(16)	1117(18)	62(2)	0.5
F(6)	8503(14)	6669(16)	568(18)	62(2)	0.5
F(7)	7914(15)	5917(17)	761(19)	62(2)	0.5
F(8)	6995(14)	7500	−832(9)	78(5)	0.5
F(9)	7801(17)	7500	2440(26)	54(5)	0.25

[a] Equivalent isotropic *U* defined as one-third of the trace of the orthogonalized $\mathbf{U}_{ij}$ tensor. [b] Site occupancy factor.

Table 3. Bond Lengths and Bond Angles in $F(cis\text{-}OsO_2F_3)_2^+Sb_2F_{11}^-$

Bond Lengths (Å)[a]					
Os(1)−F(1)	1.791(10)	[1.821]	Os(1)−F(2)	1.765(10)	[1.813]
Os(1)−O(1)	1.730(10)	[1.750]	Os(1)−O(2)	1.653(12)	[1.676]
Os(1)−F(3)	2.086(3)				
Sb(1)−F(4)	1.848(19)		Sb(1)−F(5)	1.855(18)	
Sb(1)−F(6)	1.836(18)		Sb(1)−F(7)	1.885(19)	
Sb(1)−F(8)	1.834(11)	[1.852]	Sb(1)−F(9)	2.025(29)	

Bond Angles (deg)			
F(1)−Os(1)−F(2)	86.6(4)	F(1)−Os(1)−O(1)	160.2(5)
F(2)−Os(1)−O(1)	90.2(4)	F(1)−Os(1)−O(2)	98.4(6)
F(2)−Os(1)−O(2)	99.2(5)	O(1)−Os(1)−O(2)	101.4(6)
F(1)−Os(1)−F(3)	80.2(6)	F(2)−Os(1)−F(3)	91.3(6)
O(1)−Os(1)−F(3)	80.4(5)	O(2)−Os(1)−F(3)	169.3(4)
F(2)−Os(1)−F(2a)	161.2(10)	F(3)−Os(1)−F(2a)	70.2(6)
F(2a)−Os(1)−F(3a)	91.3(6)	Os(1)−F(3)−Os(1a)	155.2(8)
F(4)−Sb(1)−F(7)	170.8(9)	F(4)−Sb(1)−F(8)	94.1(7)
F(7)−Sb(1)−F(8)	94.8(7)	F(4)−Sb(1)−F(9)	90.3(7)
F(7)−Sb(1)−F(9)	81.2(7)	F(8)−Sb(1)−F(9)	170.8(9)
F(4)−Sb(1)−F(5a)	89.5(8)	F(7)−Sb(1)−F(5a)	87.8(8)
F(8)−Sb(1)−F(5a)	93.1(8)	F(9)−Sb(1)−F(5a)	95.0(8)
F(4)−Sb(1)−F(6a)	89.1(8)	F(7)−Sb(1)−F(6a)	92.7(8)
F(8)−Sb(1)−F(6a)	92.7(8)	F(9)−Sb(1)−F(6a)	79.3(9)
F(5a)−Sb(1)−F(6a)	174.2(9)	Sb(1)−F(9)−Sb(1a)	157.7(12)

[a] Distances after correction for thermal motion by the riding model are given in square brackets.

(33) Mercier, H. P. A.; Schrobilgen, G. J. *Inorg. Chem.* **1993**, *32*, 145.
(34) Björgvinsson, M.; Mercier, H. P. A.; Mitchell, K. M.; Schrobilgen, G. J.; Strohe, G. *Inorg. Chem.* **1993**, *32*, 6046.
(35) Christe, K. O.; Dixon, D. A.; Mercier, H. P. A.; Sanders, J. C. P.; Schrobilgen, G. J.; Wilson, W. W. *J. Am. Chem. Soc.* **1994**, *116*, 2850.

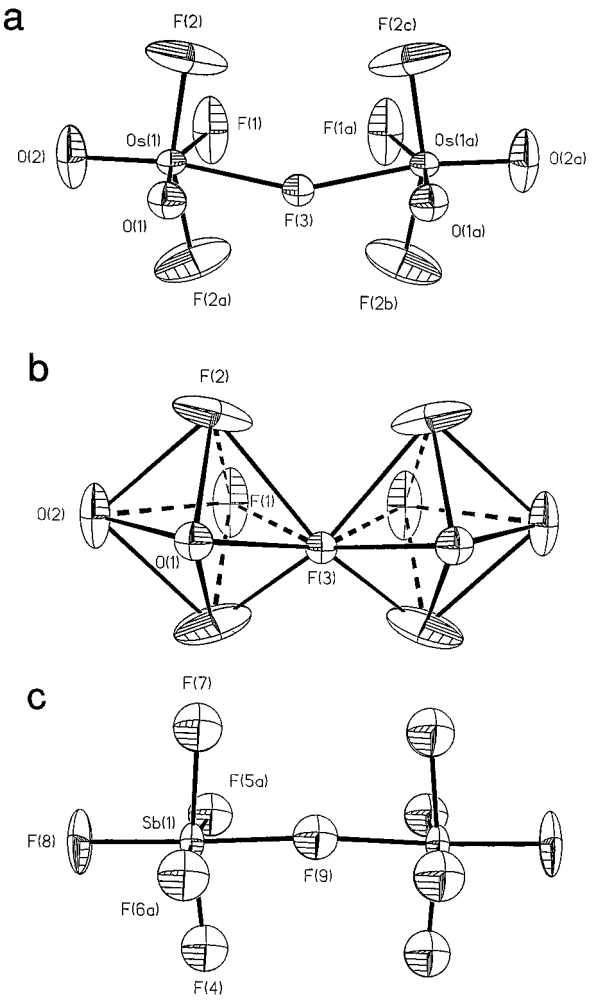

Figure 2. (a) Structure of the F(*cis*-$OsO_2F_3)_2^+$ cation in F(*cis*-$OsO_2F_3)_2{}^+Sb_2F_{11}^-$ (thermal ellipsoids at the 50% probability level); (b) octahedra formed by the light atoms surrounding the osmium atoms in the F(*cis*-$OsO_2F_3)_2^+$ cation; (c) Structure of the $Sb_2F_{11}^-$ anion in F(*cis*-$OsO_2F_3)_2{}^+Sb_2F_{11}^-$ (thermal ellipsoids at the 50% probability level).

minimal, and because anisotropic parameters for F(3) are not available, the corrected value for the Os(1)−F(3) bond length is not reported.

Until recently, there were no examples of accurately determined Os(VIII)−F and Os(VIII)−O bond lengths with which to compare bond distances in the present structure. Although average bond lengths have been determined by EXAFS spectroscopy in OsO_3F_2, $Cs_2OsO_4F_2$, and $KOsO_3F_3$ [Os(VIII)−F: 1.89(2) Å, OsO_3F_2; 2.09(2) Å, $Cs_2OsO_4F_2$; 2.05(2) and 1.92(2) Å, $KOsO_3F_3$. Os(VIII)−O: 1.70(2) Å in all three compounds],[27] the most accurate values have been determined for *cis*-OsO_2F_4 by electron diffraction,[31] for OsO_4 by electron[15] and X-ray diffraction,[17] and for the infinite-chain polymer OsO_3F_2 by X-ray diffraction.[26] The compound *cis*-OsO_2F_4 has also been studied by X-ray diffraction,[26] but owing to positional disorder among oxygen and fluorine atoms, the bond lengths reported are only average values. Like F(*cis*-$OsO_2F_3)_2^+$, *cis*-OsO_2F_4 and OsO_3F_2 contain Os(VIII) atoms which are octahedrally coordinated to oxygen and fluorine, and are chosen for comparison in this discussion.

The F(*cis*-$OsO_2F_3)_2^+$ cation exhibits a *cis*-dioxo arrangement about each osmium atom, similar to that observed in *cis*-OsO_2F_4.[31] The preference for the *cis*-dioxo-bonded structure can be understood in terms of the relative spatial orientations of the strong π-donor oxygen p orbitals and the approximately $d_{t_{2g}}$ orbitals of osmium required for $p_\pi \rightarrow d_\pi$ bonding. The "*cis*-dioxo effect" has been noted previously in molybdenum(VI) and tungsten(VI) dioxofluoro compounds[36,37] and in the $[TcO_2F_4]$ unit of TcO_2F_3.[33] Each oxygen atom of a [*cis*-OsO_2F_4] unit possesses two filled p orbitals available for π-bonding with an empty set of osmium t_{2g} orbitals. If the oxygens were *trans*, the two donating p orbitals on both oxygen atoms would compete for the same two $d_{t_{2g}}$ orbitals having the correct symmetry for overlap whereas, in the *cis* isomer, all three $d_{t_{2g}}$ orbitals are available for overlap. Consequently, the bonding molecular orbitals in the *cis* isomer have lower energies than the corresponding molecular orbitals in the *trans* isomer, providing greater stability for the *cis* isomer.

The preference for fluorine bridging *trans* to oxygen atoms in F(*cis*-$OsO_2F_3)_2^+$ and related structures is attributed to the *trans* influence of the doubly bonded oxygen atoms. In a valence-bond description of the F(*cis*-$OsO_2F_3)_2^+$ cation (structures **I**−**III**) and related fluorine-bridged structures, the bridging

$$F_3O_2OsF\ {}^+OsO_2F_3 \leftrightarrow F_3O_2Os^+\ F^-\ OsO_2F_3 \leftrightarrow$$
I **II**

$$F_3O_2Os^+\ FOsO_2F_3$$
III

fluorine bears more negative charge than the terminal fluorines and the Os---F bridge bond length (2.086(3) Å), which is significantly longer than the terminal Os−F bond distances, is in good agreement with the bridging Os---F bond distances in OsO_3F_2 (2.126(1) and 2.108(1) Å). Because fluorine is a poorer π-donor than oxygen, the negative charge on the bridging fluorine is reinforced when the strong π-donor oxygen atom *trans* to the fluorine bridge competes for the same two $d_{t_{2g}}$ orbitals. This leads to a negligible $p_\pi \rightarrow d_\pi$ contribution from the bridging fluorine and a further enhancement of negative charge on the bridging fluorine. Because all three $d_{t_{2g}}$ orbitals are available for overlap with fluorine p orbitals of appropriate symmetry, the terminal fluorines *cis* to the oxygens and *trans* to each other are less basic and are not favored for bridge formation in F(*cis*-$OsO_2F_3)_2^+$ and related fluorine-bridged *cis*-dioxo structures such as TcO_2F_3[33] and OsO_3F_2.[26]

There are two sets of Os−O and terminal Os−F bonds in the F(*cis*-$OsO_2F_3)_2^+$ cation, those *trans* to a terminal F ligand and those *trans* to the bridging F ligand. The Os−O bonds *trans* to terminal fluorines (1.750 Å) are considerably longer than the Os−O bonds *trans* to the fluorine bridge (1.676 Å) and the Os−O bond lengths in *cis*-OsO_2F_4 (1.674(4) Å).[31] In contrast to Os−F bonding, a significant contribution to Os−O bonding is made by $p_\pi-d_\pi$ interactions between ligand filled 2p orbitals and empty metal d_{xy}, d_{xz}, and d_{yz} orbitals. The d orbitals in the more electronegative Os(VIII) cation are more contracted and, hence, less available for $p_\pi-d_\pi$ interaction than the d orbitals of neutral *cis*-OsO_2F_4. This weaker π-bonding interaction accounts for the longer Os−O(1) bond (1.750 Å) *trans* to F(1) in the cation than in the neutral species (1.674(4) Å). The Os−O bonds *cis* to the fluorine bridge in F(*cis*-$OsO_2F_3)_2^+$ and OsO_3F_2 (1.727(1) Å) are, in fact, the longest Os−O bonds known and are significantly longer than the Os−O bond length reported for OsO_4 (1.7105(5)−1.711(3) Å).[17] The Os−O(2) bond of F(*cis*-$OsO_2F_3)_2^+$ is *trans* to the bridging F(3)

(36) Arnaudet, L; Bougon, R.; Ban, B.; Charpin, P.; Isabey, J.; Lance, M.; Nierlich, M.; Vigner, J. *Can. J. Chem.* **1990**, *68*, 507.
(37) (a) Buslayev, Yu. A.; Kokunov, Yu. V.; Bochkaryova, V. A.; Shustorovich, E. M. *J. Inorg. Nucl. Chem.* **1972**, *34*, 2861 and references therein. (b) Buslaev, Yu. A.; Kokunov, Yu. V.; Bochkareva, V. A.; Shustorovich, E. M. *Russ. J. Inorg. Chem. (Engl. Transl.)* **1972**, *17*, 1675 and references therein.

ligand and has a bond length of 1.676 Å, which is essentially identical to the Os−O bond length in *cis*-OsO_2F_4 (1.674(4) Å).[31] As already noted, the bridging F(3) ligand competes less effectively for the empty metal d orbitals than the terminal F ligands in the cation and in the neutral molecule. This allows for a greater share of the contracted d orbitals in the cation to be available for $p_\pi-d_\pi$ interaction between Os and the O(2) ligand *trans* to F(3) and accounts for the shortening of the Os−O(2) bond relative to the Os−O(1) bond *trans* to the terminal F(1) ligand. In OsO_2F_3, the Os−O bond lengths *trans* to the fluorine bridges (1.683(1) Å) and the Os−O bond lengths *trans* to the terminal fluorines (1.727(1) Å)[26] are similar to those in F(*cis*-$OsO_2F_3)_2^+$. The Os atom of the F(*cis*-$OsO_2F_3)_2^+$ cation is expected to be more electronegative, having stronger, shorter σ-bonds than in *cis*-OsO_2F_4. The terminal Os−F bonds are slightly shorter in F(*cis*-$OsO_2F_3)_2^+$ (1.813 and 1.821 Å) than in *cis*-OsO_2F_4 (1.843(3) and 1.883(3) Å)[31] and may be accounted for in terms of a reduction in Os−F bond polarities arising from the formal positive charge associated with each osmium atom in resonance structures **I**−**III**. The terminal Os−F(1) bond length *trans* to O(1) in F(*cis*-$OsO_2F_3)_2^+$ (1.821 Å) and the Os−F_{eq} bond in *cis*-OsO_2F_4 (1.883(3) Å)[31] are significantly longer than the *trans* Os−F(2) bonds in F(*cis*-$OsO_2F_3)_2^+$ (1.813 Å) and in *cis*-OsO_2F_4 (1.843(3) Å).[31] The lengthening of terminal Os−F bonds *trans* to oxygen relative to Os−F bonds that are *trans* to one another is attributed to the *trans* influence of the oxygen atoms and is also observed for the [OsO_3F_3], [TcO_2F_4], [$MoOF_5$], and [$ReOF_4$] units of the infinite-chain polymers OsO_3F_2,[26] TcO_2F_3,[33] $MoOF_4$,[38] and $ReOF_4$,[39] the [WOF_5] unit of tetrameric WOF_4,[40] and the [$TcOF_5$] unit of trimeric $TcOF_4$,[41] where the fluorine bridges also occur *trans* to the oxygens.

The light atoms in the F(*cis*-$OsO_2F_3)_2^+$ cation form two corner-shared octahedra related by a 2-fold axis (Figure 2b). Although there is considerable variation in the bond lengths around each osmium atom, the octahedra formed by the light atoms are relatively undistorted, as shown by the ranges of the nearest neighbor−ligand atom contacts: F···F, 2.44(1)−2.51(2), F···O, 2.48(2)−2.61(2), O···O, 2.62(2) Å. The eccentricity of the osmium atom within the light-atom octahedron is described relative to the three orthogonal planes of this octahedron. The two oxygen atoms and the *trans* fluorine atoms of the [OsO_2F_4] unit describe one of these planes, namely, the [O(1), O(2), F(1), F(3)] plane. The deviation of the Os atom from this plane is only 0.032(6) Å, showing that the Os atom can be regarded as lying in this plane. The osmium atom also lies in a second orthogonal plane, [O(2), F(2), F(2a), F(3)], with a deviation of 0.098(9) Å. The Os atom does not lie in the third orthogonal plane, [O(1), F(2), F(2a), F(1)], but is displaced 0.522(7) Å from the latter plane toward the oxygen atoms in the [O(1), O(2), Os(1), F(1), F(3)] plane. This displacement is significantly larger than displacements observed in *cis*-OsO_2F_4 (0.129 Å),[31] $MoOF_4$ (0.31 Å),[38] WOF_4 (0.30 Å),[40] $ReOF_4$ (0.30 Å),[39] and TcO_2F_3 (0.22−0.26 Å)[33] with the largest previously reported value being 0.36 Å for the $TcOF_4$ trimer.[41] Although the *cis* fluorines of each [OsO_2F_4] unit of the F(*cis*-$OsO_2F_3)_2^+$ cation are related by symmetry, the angles about the Os atom are not imposed by symmetry and are comparable to those found in *cis*-OsO_2F_4 [31] and OsO_3F_2.[26] The osmium atom displacements within the light-atom octahedra are also reflected in the angles the light atoms form with the osmium atoms and can be rationalized in terms of the VSEPR rules.[42] The greater spatial requirements of oxygen-double-bond domains and their repulsive interactions with neighboring electron bond pair domains cause the angles subtended at osmium by the bridging fluorine and terminal fluorine atoms and O(1) to be significantly less than 90° [F(1)−Os−F(3) 80.2(6)°, F(2)−Os−F(3) 80.8(6)°, O(1)−Os−F(3) 80.4(4)°] so that the OsO_2F_3 moieties bridged to F(3) are essentially square pyramids in which the osmium atom is located above the [O(1), F(1), F(2), F(2a)] plane and is predominantly displaced toward O(2). Because the distortions about osmium largely occur about the O(2)−Os−F(3) axis, the O(1)−Os−F(2) (90.2(4)°) and F(1)−Os−F(2) (86.6(4)°) angles suffer the least distortion, whereas angles lying along [O(2)−Os−F(3) 169.3(4)°] and perpendicular to [O(1)−Os−F(1) 160.2(5)°, F(2)−Os−F(2a) 161.2(10)°] the O(2)-Os−F(3) axis suffer larger distortions. These distortions are presumably heightened by the smaller spatial requirement of the longer Os−F(3) bridge bond domain *trans* to O(2) and are associated with the greater eccentricity of the osmium atom in the diosmium cation than in *cis*-OsO_2F_4. Moreover, the F(2)−Os−F(2a) angle (161.2(10)°) is bent away from the *cis*-oxygen bond pair domains toward the *cis*-fluorine bridge and is significantly smaller than the corresponding angle in *cis*-OsO_2F_4 (172.0-(35)°).[31]

The bridge bond angles of the cation and anion reflect the type of close packing adopted by the light atoms in the structure. Edwards and co-workers[38−41] have shown that a hexagonally close-packed structure with metal atoms in octahedral sites has an ideal angle at the fluorine bridge atom of 132°, whereas for cubic close packing this angle is 180° (cf. ref 43)). The bond angle at the bridging fluorine atom of the F(*cis*-$OsO_2F_3)_2^+$ cation [Os(1)−F(3)−Os(1a)] is 155.2(8), and that for $Sb_2F_{11}^-$ [Sb(1)−F(9)−Sb(1a)] is 158(1)°, intermediate between hexagonal and cubic close packing. The shortest interionic contact distances are all within the range 2.52(2)−2.91(2) Å, also consistent with close packing of the light atoms; cf. van der Waals contacts F···F = 2.70 Å and F···O = 2.75 Å.[44]

The $Sb_2F_{11}^-$ anion is also subject to a positional disorder, and in this case, it was possible to define a model resulting from the superposition of two anions in which the central Sb atoms occupy identical positions. One of these anions is shown in Figure 2c. The ellipsoid of the terminal fluorine (F(8)) *trans* to the fluorine bridge, for which the disorder could not be resolved, has the same characteristic impeller shape as those observed for the light atoms in the F(*cis*-$OsO_2F_3)_2^+$ cation (*vide supra*). The librationally corrected Sb−F(8) bond distance is given in Table 3. The presence of disorder on both the bridging fluorine and the equatorial fluorine atoms gives rise to two possible geometric conformations for the $Sb_2F_{11}^-$ anion where the dihedral angle between the two sets of equatorial planes of each SbF_6 unit sharing the bridging fluorine atom, ψ, is either 35.4 or 8.3°. The choice of the correct conformation was based on a well-documented correlation between the M---F_b---M bridging angle and ψ.[45] An increase in the dihedral angle, ψ, serves to minimize steric repulsions between the nearest-

(38) Edwards, A. J.; Steventon, B. R. *J. Chem. Soc. A* **1968**, 2503.
(39) Edwards, A. J.; Jones, J. R. *J. Chem. Soc. A* **1968**, 2511.
(40) Edwards, A. J.; Jones, J. R. *J. Chem. Soc. A* **1968**, 2074.
(41) Edwards, A. J.; Jones, J. R., Sills, R. J. *J. Chem. Soc. A* **1970**, 2521.
(42) Gillespie, R. J.; Hargittai, I. *The VSEPR Model of Molecular Geometry*; Allyn and Bacon: Boston, 1991.
(43) The structure of $F(ReOF_4)_2^+Sb_2F_{11}^-$ [8] shows approximate cubic close packing of light atoms and has a bridging angle of 170(3)° for $F(ReOF_4)_2^+$ and 179(5)° for $Sb_2F_{11}^-$. In contrast, in the structure of $H_3O^+W_2O_2F_9^-$ (Hoskins, B. F.; Linden, A.; O'Donnell, T. A. *Inorg. Chem.* **1987**, *26*, 2223), the bond angle at the bridging fluorine atom of the $W_2O_2F_9^-$ anion is 144(2)°, indicating an arrangement closer to hexagonal close packing.
(44) Pauling, L. *The Nature of the Chemical Bond*, 3rd ed.; Cornell University Press: Ithaca, NY, 1960; p 260.
(45) (a) Burgess, J.; Fraser, C. J. W.; McRae, V. M.; Peacock, R. D.; Russell, D. R. *Inorg. Nucl. Chem. Suppl.* **1976**, 183. (b) Bruce, D. M.; Holloway, J. H.; Russell, D. R. *J. Chem. Soc., Dalton Trans.* **1978**, 1627.

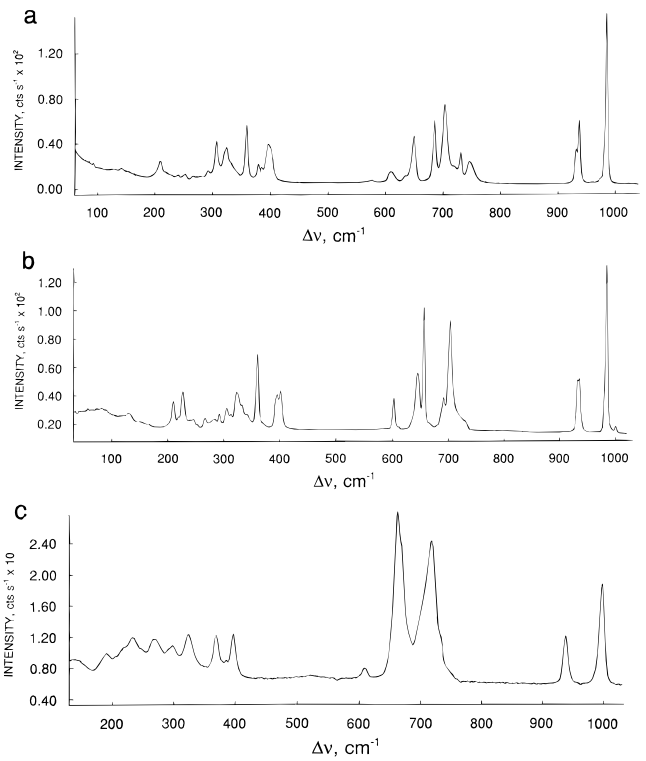

Figure 3. Raman spectra of (a) microcrystalline F(*cis*-$OsO_2F_3)_2^+AsF_6^-$ recorded under a layer of liquid HF/AsF_5 at −70 °C in an FEP sample tube, (b) microcrystalline F(*cis*-$OsO_2F_3)_2^+Sb_2F_{11}^-$ recorded at −110 °C in a 3-mm-o.d. Pyrex sample tube, and (c) a solution of $OsO_2F_3^+Sb_nF_{5n+1}^-$ in SbF_5 solvent recorded in a $^1/_4$-in.-o.d. FEP reactor at 23 °C, using 647.1-nm excitation.

neighbor fluorine atoms of each octahedron as the M---F_b---M angle decreases. The dihedral angle is 0° when M---F_b---M is linear, reaching a maximum of 45° when M---F_b---M is *ca.* 145°. An examination of a plot of ψ versus M---F_b---M angle shows that a value of 35.4° for ψ would be expected for a M---F_b---M angle of ∼147°, while a value of 8.3° is in the range expected for the experimentally determined bridge angle of 155° and leads to the choice of the latter angle.

The Sb−F bond lengths found in the present case are similar to those reported previously.[46] The longer bridging Sb−F bonds have the usual effect of distorting the octahedral environments around the antimony atoms. The four fluorine atoms F(4), F(7), F(5a), and F(6a) are coplanar with a maximum deviation of 0.028 Å; however, the plane is displaced 0.11 Å toward the bridge bond and away from the Sb atom.

Raman Spectroscopy and Vibrational Assignments. (a) The F(*cis*-$OsO_2F_3)_2^+$ Cation. The low-temperature Raman spectra of solid F(*cis*-$OsO_2F_3)_2^+AsF_6^-$ precipitated from AsF_5/HF solution at −70 °C and solid F(*cis*-$OsO_2F_3)_2^+Sb_2F_{11}^-$ are shown in Figures 3a,b. The observed frequencies along with their assignments are given in Table 4. Vibrational assignments of the cation were made under C_s symmetry. In the cation, F_a denotes the four terminal fluorines (two on each osmium atom) that are *trans* to one another, F_t denotes the two terminal fluorine atoms (one on each osmium atom) *trans* to oxygen atoms, and F_b denotes the bridging fluorine atom. The four oxygen atoms are labeled as O_b or O_t, depending on whether they are *trans* to the bridging fluorine (F_b) or a terminal fluorine (F_t), respectively. A maximum of 33 bands ($\Gamma = 21A' + 12A''$) is expected for the vibrational spectrum of the cation; these include the symmetric and asymmetric Os_2F_b bridging stretching modes, Os---F_b---Os bridge bend, and remaining bends and torsions associated with the fluorine bridge. Moreover, all bands are expected to be Raman-active under C_s or lower point symmetry. Assignments of the cation modes were made by comparison with the known transition metal *cis*-dioxo species, *cis*-OsO_2F_4,[31] *cis*-$ReO_2F_4^-$,[47] and the *cis*-TcO_2F_4 unit of polymeric TcO_2F_3,[33] as well as with *cis*-$IO_2F_4^-$,[48] and were confirmed by local (LDFT) and nonlocal (NLDFT) density functional theory calculations (see Table 4 and **Computational Results**). Assignments of anion modes are based on published data for the $Sb_2F_{11}^-$ [49−53] and AsF_6^- [49,52,54] anions.

A factor-group analysis correlating the $C_s(xz)$ point symmetry of the free cation to the crystallographic site symmetries of the two osmium atoms $C_s(xz)$ and the bridging fluorine ($C_s(xz)$) to the symmetry of the unit cell (D_{2h}) reveals that vibrational coupling within the unit cell should, in principle, lead to splitting of the bands in the vibrational spectra of the F(*cis*-$OsO_2F_3)_2^+$ cation. Vibrational bands belonging to the A′ representation, i.e., $\nu_1-\nu_{21}$, should be split into Raman-active A_g and B_{2g} components and infrared-active B_{1u} and B_{3u} components. Vibrational bands belonging to the A″ representation, i.e, $\nu_{22}-\nu_{33}$, are predicted to be split into Raman-active B_{1g} and B_{3g} components, an infrared-active B_{2u} component, and a Raman- and infrared-inactive A_u component. In the majority of cases, the factor-group splittings predicted in the Raman spectrum of F(*cis*-$OsO_2F_3)_2^+$ are apparently too small to be resolved. A number of weak shoulders associated with the Os−O stretching modes may be attributable to the B_{2g} components, which are expected to be less intense than their A_g components.

The highest frequency bands in the spectra of the AsF_6^- and $Sb_2F_{11}^-$ salts of the F(*cis*-$OsO_2F_3)_2^+$ cation are assigned to stretches involving the Os−O double bonds. Typically, in *cis*-dioxo systems, these bands are assigned as the symmetric and asymmetric stretches of the MO_2 moiety. In the dimer cation, the Os−O bonds are no longer equivalent. The Os−O_b bonds are stronger and shorter than the Os−O_t bonds; and the vibrational modes associated with the two Os−O_b bonds are expected to occur at higher frequencies than those associated with the Os−O_t bonds. Consequently, the higher frequency and more intense bands at 986/984 cm^{-1} along with shoulders at 982, 975/980 cm^{-1} in the $AsF_6^-/Sb_2F_{11}^-$ salts are assigned to the symmetric and asymmetric stretches, respectively, of the Os−O_b bonds. The lower intensity bands at 938/936 and 933/933 cm^{-1} are assigned to the asymmetric and symmetric stretches, respectively, of the Os−O_t bonds.

An intense band occurring in the spectra of both the AsF_6^- and $Sb_2F_{11}^-$ salts is observed at 703 cm^{-1} with weaker bands at 731, 720/730 cm^{-1}, respectively; these are assigned to the OsF_{2a} stretches. The more intense band is assigned to ν_{sym}(OsF_{2a}), while the weaker and higher frequency bands are assigned to ν_{as}(OsF_{2a}). These bands show the same relative frequency ordering as the analogous modes for *cis*-$IO_2F_4^-$,[48] the TcO_2F_4 unit of TcO_2F_3,[33] and *cis*-OsO_2F_4[31] and occur at higher frequency than the OsF_{2a} stretches of *cis*-OsO_2F_4 (ν_{as}-

(46) (a) Davies, C. G.; Gillespie, R. J.; Ireland, P. R.; Sowa, J. M. *Can. J. Chem.* **1974**, *52*, 2048. (b) McKee, D. E.; Zalkin, A.; Bartlett, N. *Inorg. Chem.* **1973**, *12*, 1713.

(47) Kuhlmann, W.; Sawodny, W. *J. Fluorine Chem.* **1977**, *9*, 341.
(48) Christe, K. O.; Wilson, R. D.; Schack, C. J. *Inorg. Chem.* **1981**, *20*, 2104.
(49) Gillespie, R. J.; Schrobilgen, G. J. *Inorg. Chem.* **1974**, *13*, 1230.
(50) Boldrini, P.; Gillespie, R. J.; Schrobilgen, G. J. *Inorg. Chem.* **1974**, *13*, 1690.
(51) Gillespie, R. J.; Landa, B.; Schrobilgen, G. J. *Inorg. Chem.* **1976**, *15*, 1256.
(52) Gillespie, R. J.; Schrobilgen, G. J. *Inorg. Chem.* **1976**, *15*, 22.
(53) Chen, G. S. H.; Passmore, J. *J. Chem. Soc., Dalton Trans.* **1979**, 1251.
(54) Barraclough, C. G.; Besida, J.; Davies, P. G.; O'Donnell, T. A. *J. Fluorine Chem.* **1988**, *38*, 405.

Table 4. Experimental and Calculated Raman Frequencies, Assignments, and Mode Descriptions for $F(cis\text{-}OsO_2F_3)_2^+$

freq (cm^{-1})				
exp[b]		$F(cis\text{-}OsO_2F_3)_2^+$ [a]		
$F(cis\text{-}OsO_2F_3)_2^+AsF_6^-$	$F(cis\text{-}OsO_2F_3)_2^+Sb_2F_{11}^-$	LDFT[c]	NLDFT	assigns, C_s point symm
986 (100)	984 (100) 1000 (6)	1049 (0.1) {986}	1031 (77)	A′, $\nu_{sym}(OsO_b)$
982 sh	980 sh	1045 (155) {982}	1023 (178)	A″, $\nu_{as}(OsO_b)$
975 sh				
938 (33)	936 (33)	997 (30) {937}	959 (19)	A″, $\nu_{as}(OsO_t)$
933 (18)	933 (33)	990 (49) {931}	940 (32)	A′, $\nu_{sym}(OsO_t)$
731 (23)	730 (7)	749 (114) {704}	783 (68)	A″, $\nu_{as}(OsF_{2a})$
720 sh				
703 (45)	703 (60)	754 (202) {709}	784 (158)	A′, $\nu_{sym}(OsF_{2a})$
650 (25)	645 (35)	706 (52) {664}	725 (132)	A′, $\nu_{sym}(OsF_t + OsF_{2a})$
635 sh		701 (44) {659}	720 (116)	A″, $\nu_{as}(OsF_t + OsF_{2a})$
610 (6)	611 (3)	634 (18) {596}	640 (36)	A′, $\nu_{sym}(OsF_t - OsF_{2a})$
		635 (52) {597}	633 (12)	A″, $\nu_{as}(OsF_t - OsF_{2a})$
492 (<1)	495 (<1)	494 (207)	649 (197)	A″, $\nu_{as}(Os\text{---}F_b\text{---}Os)$
401 (18)	404 sh 402 (25)	431 (118)	439 (2.5)	A′, $\delta_{sym}(Os'O_2 + OsO_2)$
396 (20)	395 (22) 392 sh	427 (4.2)	429 (4.1)	A″, $\delta_{as}(Os'O_2 - OsO_2)$
359 (30)	360 (45)	415 (0.4)	392 (4.0)	A′, $\delta_{sym}(F_tOsF_a - F_tOsF_a)$
		410 (29)	391 (0.7)	A″, $\delta_{as}(F_tOsF_a - F_tOsF_a)$
		406 (0.1)	360 (11)	A′, $\delta_{sym}(Os_2F_b$ toward $F_t)$
		402 (5.9)	352 (2.8)	A′, $\delta_{sym}(Os_2F_b$ toward $F_a + F_aOsF_b)$
		392 (4.2)	338 (9.7)	A″, $\delta_{as}(F_a\ OsF_b)$
		370 (29)	330 (18)	A′, $\delta_{sym}(F_a\ OsF_b)$
343 sh	341 (10)	366 (1.1)	311 (10)	A″, $\delta_{as}(F_a\ OsO_t)$ + other bends
332 sh	333 (16)	358 (128)	306 (6.8)	A′, $\delta_{sym}(F_a\ OsO_t)$ + other bends
325 (18)	323 (23)	342 (0.5)	294 (50)	A′, $\delta_{sym}(OsF_{2a}$ toward $F_b)$
321 sh				
307 (22)	313 (10) 305 (15)	326 (8.9)	281 (5.2)	A′, $\delta_{sym}(OsF_{2a}$ toward $O_t)$
292 (5)	292 (10)	286 (3.9)	268 (1.5)	A′, $\delta_{sym}(O_tOsF_t$ toward $F_a)$
279 (2)	283 (6)	284 (5.5)	236 (9.2)	A′, $\delta_{sym}(O_tOsF_t$ toward $F_a + Os_2F_b)$
253 (3)	252 (2)	263 (3.2)	167 (0.3)	A′, $\delta_{sym}(O_tOsF_t - OsF_{2a})$
	246 (6)	258 (7.8)	164 (0.6)	A″, $\delta_{as}(OsF_{2a}$ toward $F_b - F_tOsF_b)$
240 (2)	241 (5)			
228 (2)	228 (24)	193 (3.6)	158 (1.2)	A′, $\delta_{sym}(OsF_{2a}$ toward $F_b - F_tOsF_b)$
209 (10)	210 (17)	190 (0.4)	140 (0.3)	A′, $\delta_{sym}(O_t$ rocks toward $O_t')$
154 (2)	152 (2)	177 (2.8)	108 (2.7)	A′, $\delta_{sym}(F_{2a}$ rocks toward $F_{2a}')$
142 (3)		131 (0.3)	103 (1.0)	A″, $\delta_{as}(F_{2a}$ rocks toward $F_{2a}')$
128 (2)	131 (6)	120 (13)	58 (0.3)	A′, $\delta_{sym}(F_{2a}$ rocks toward $F_t')$
92 (3)	93 (12)	109 (5.0)	22 (0.6)	A′, torsion about Os---Fb---Os
747 (12)				AsF_5[d]
685 (32)				$\nu_1(A_{1g})$, AsF_6^-
672 sh				
576 (2)				$\nu_2(E_g)$, AsF_6^-
385 (9)				$\nu_4(T_{1u})$, AsF_6^-; $\nu_5(T_{2g})$, AsF_6^-
373 (12)				
	691 (23)			$Sb_2F_{11}^-$
	679 (2)			
	665 (6)			
	656 (70)			
	602 (22)			
	120 (3)			lattice modes
	104 (1)			

[a] Infrared intensities in km mol^{-1} are given in parentheses. [b] Values given in parentheses are Raman intensities. [c] The stretching frequencies were scaled by an empirical factor of 0.94 (values enclosed in braces) to maximize their agreement with the observed values (see ref 31). [d] The band is assigned to excess AsF_5 present in the HF supernatant under which the solid was recorded. The $\nu_1(A'_1)$ mode for AsF_5 in the gas phase occurs at 733 cm^{-1} (Hoskins, L. C.; Lord, R. C. *J. Chem. Phys.* **1967**, *46*, 2402).

(OsF_{2a}) 680 cm^{-1}; $\nu_{sym}(OsF_{2a})$ 673 cm^{-1}). High-frequency shifts relative to *cis*-OsO_2F_4 are expected for the cation, because the Os−F bonds are expected to be shorter and less polar, as may be inferred from resonance structures **I**−**III** (also see **X-ray Crystal Structure**). In the absence of a large π-bonding interaction, bond energies of transition metals bonded to electronegative elements are expected to decrease as the metals become more electropositive and the bonds become more ionic. This is observed for the M−F_a bonds with $\nu_{sym}(MF_{2a})$[55] showing a significant decrease over the following isoelectronic series: *cis*-OsO_2F_4, 673 cm^{-1};[31] *cis*-$ReO_2F_4^-$, 647 cm^{-1};[47] *cis*-$WO_2F_4^{2-}$, 588 cm^{-1} [56] (potassium salts).

Although the Raman spectra of both salts are complicated in the regions 600−700 cm^{-1} and below 400 cm^{-1} by bands arising from the anions, the bands at 650/645 and 610/611 cm^{-1} are common to both the AsF_6^- and $Sb_2F_{11}^-$ salts. These bands are assigned to the in-phase and out-of-phase components of the coupled $\nu_{sym}(Os-F_t \pm OsF_{2a})$ stretching modes based on the calculated frequencies for these modes. The pure Os−F_t stretching modes and their coupled counterparts are expected

(55) Described as the symmetric combination of symmetric axial and symmetric equatorial OsF_2 stretches in *cis*-OsO_2F_4.

(56) Mattes, R.; Müller, G.; Becher, H. J. *Z. Anorg. Allg. Chem.* **1972**, *389*, 177.

to occur at lower frequencies than observed for $\nu_{sym}(OsF_{2a})$ as a result of the *trans* influence of the doubly bonded oxygen ligands. Similar frequency differences arising from the *trans* influence of oxygen are observed for $\nu_{as}(Os-F_t \pm OsF_{2a})$ and $\nu_{as}(OsF_{2a})$ as well as for $\nu_{as}(MF_{2t})$ and $\nu_{as}(MF_{2a})$ in the spectra of *cis*-OsO_2F_4 (571, 680 cm^{-1}),[31] *cis*-$ReO_2F_4^-$ (489, 606 cm^{-1}),[47] *cis*-$WO_2F_4^{2-}$ (468, 555 cm^{-1}),[56] and *cis*-$MoO_2F_4^{2-}$ (453, 555 cm^{-1})[56] (potassium salts). The asymmetric Os---F_b---Os bridging stretching mode is tentatively assigned to broad, weak bands at 492/495 cm^{-1}. In d^0 transition metal fluoro complexes involving bridging fluorine atoms, frequencies of stretching modes involving a bridging fluorine atom are usually ca. 200 cm^{-1} lower than stretching frequencies associated with the terminal fluorine ligands;[57] the observed difference is 225/222 cm^{-1} for F(*cis*-$OsO_2F_3)_2^+$. Typically, bands involving such modes are very broad and weak in the Raman spectra. The calculated value is 650 cm^{-1} at the nonlocal level and 494 cm^{-1} at the local level and is more in accord with the observed feature. However, it should be noted that the calculated frequencies are for a single structure at the minimum of the potential energy surface. The cation has a number of low-energy modes (100−200 cm^{-1}) involving motions of the OsO_2F_3 groups. Thus, these groups will be found in a variety of positions and the bridging fluorine will experience a variety of different potentials. This will lead to significant broadening of the peak associated with the asymmetric stretch. The symmetric Os---F_b---Os stretch, while expected to occur at lower frequency and to be more intense than its asymmetric counterpart, has not been assigned (see **Computational Results**).

The low symmetry of the diosmium cation allows for considerable mixing of the bending modes (see Table 4). The assignments for the bending region are made by comparison with other *cis*-dioxo complexes and do not take into account all possible mixing. The two medium-intensity bands at 401 and 396 cm^{-1} for the AsF_6^- salt and split bands at 404, 402 cm^{-1} and 395, 392 cm^{-1} in the $Sb_2F_{11}^-$ salt are assigned to the in-phase and out-of-phase components of OsO_2 scissors modes by comparison with the analogous modes for polymeric TcO_2F_3 (411 cm^{-1}),[33] *cis*-OsO_2F_4 (402 cm^{-1}),[31] *cis*-$ReO_2F_4^-$ (410 cm^{-1}, reassigned),[47] *cis*-$WO_2F_4^{2-}$ (382 cm^{-1}),[56] *cis*-$MoO_2F_4^{2-}$ (385 cm^{-1}),[56] and *cis*-$IO_2F_4^-$ (394 cm^{-1}).[48] The bands at 359/360 cm^{-1} are similar in relative intensity to a symmetric combination of axial and equatorial OsF_2 scissors modes for *cis*-OsO_2F_4, which occurs at a slightly lower frequency (350 cm^{-1}),[31] and are assigned to unresolved symmetric and asymmetric combinations of F_tOsF_a scissors modes in the spectrum of the cation. Modes involving the bridging fluorine (F_b) are expected to be weak and broad in the Raman spectrum and are not assigned. The bands at 343/341 and 325, 321/323 cm^{-1} and at 307/313, 305 cm^{-1} have counterparts in the Raman spectrum of *cis*-OsO_2F_4 assigned to the symmetric combination of $OOsF_e$ and OsF_{2a} scissors (344 cm^{-1})[31] and the $\delta_{rock}(OsF_{2a})$ (323 cm^{-1}), respectively. Although assignments of bands below 320 cm^{-1} have also been aided by LDFT and NLDFT calculations, they must be regarded as tentative. The calculations indicate that the bands are extensively coupled and involve $OOsF_a$, OsF_{2a}, and $OOsF_t$ bends in combination with other bends and torsions (see Table 4 and **Computational Results**).

(b) The $OsO_2F_3^+$ Cation. Although a solid $OsO_2F_3^+$ salt could not be isolated from SbF_5 solution, the Raman spectrum of a solution of *cis*-OsO_2F_4 in SbF_5 is consistent with that of the $OsO_2F_3^+$ cation and is shown in Figure 3c. The solution spectrum is similar to, but simpler than, those of the AsF_6^- and $Sb_2F_{11}^-$ salts of the F(*cis*-$OsO_2F_3)_2^+$ cation. The $OsO_2F_3^+$ cation is expected to be isostructural with isoelectronic ReO_2F_3, which has been assigned under C_{2v} point symmetry as the matrix-isolated monomer.[58] Density functional theory calculations confirm that the energy-minimized structures for both $OsO_2F_3^+$ and ReO_2F_3 have C_{2v} point symmetry (structure IV).

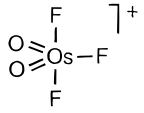

IV

Frequencies and assignments for the $OsO_2F_3^+$ cation and the ReO_2F_3 monomer are given in Table 5, and values calculated from density functional theory are discussed under **Computational Results** and are also listed in Table 5.

A total of 12 Raman-active modes are expected for $OsO_2F_3^+$ under C_{2v} point symmetry ($\Gamma = 5A_1 + A_2 + 3B_1 + 3B_2$). The two bands at 996 and 940 cm^{-1} are assigned to the symmetric and asymmetric OsO_2 stretches of the $OsO_2F_3^+$ cation, respectively, by analogy with other known *cis*-dioxo complexes (*vide supra*) and were confirmed by Raman depolarization measurements in SbF_5 solution. Larger available empty d orbitals appear to correlate with an increase in $p_\pi-d_\pi$ bonding, leading to $\nu_{sym}(MO_2)$ frequencies which overall increase on moving from *cis*-OsO_2F_4 to the isoelectronic *cis*-$ReO_2F_4^-$ and *cis*-$WO_2F_4^{2-}$ anions as the metals become progressively more electropositive. These assignments are opposite to the ordering of the corresponding modes of *cis*-$IO_2F_4^-$ ($\nu_{sym}(IO_2)$, 856 cm^{-1}; $\nu_{as}(IO_2)$, 875 cm^{-1})[48] but are consistent with assignments previously made under C_{2v} point symmetry for transition metal species where $\nu_{as}(MO_2)$ (B_2) is lower in frequency than $\nu_{sym}(MO_2)$ (A_1): e.g., *cis*-OsO_2F_4, 933, 943 cm^{-1};[31] *cis*-$ReO_2F_4^-$, 951, 987 cm^{-1};[47] *cis*-$WO_2F_4^{2-}$, 905, 962 cm^{-1};[56] *cis*-$MoO_2F_4^{2-}$, 907, 950 cm^{-1};[56] *cis*-$NbO_2F_4^{3-}$, 811, 890 cm^{-1} [59] (potassium salts). The same frequency ordering is observed for $\nu_{as}(MO_2)$ and $\nu_{sym}(MO_2)$ of related MO_2F_3-based fluorine-bridged systems: e.g., $MoO_2F_3^-$, 912, 974 cm^{-1}; and $WO_2F_3^-$, 890, 988 cm^{-1} (cesium salts).[56] As expected for the more electronegative Os(VIII) metal center in the $OsO_2F_3^+$ cation, these bands are slightly higher in frequency than the corresponding bands for F(*cis*-$OsO_2F_3)_2^+$. Interestingly, while $p_\pi-d_\pi$ interactions are expected to be weaker in the $OsO_2F_3^+$ cation and the d orbitals are expected to be more contracted than in the F(*cis*-$OsO_2F_3)_2^+$ cation, the frequency difference between the symmetric and asymmetric OsO_2 stretches is still relatively large (56 cm^{-1}), as in the related $MoO_2F_3^-$ (62 cm^{-1}) and $WO_2F_3^-$ (98 cm^{-1}) anions. This appears reasonable because the distorted trigonal bipyramidal structures expected for these anions and $OsO_2F_3^+$ place only one fluorine ligand in the equatorial plane proximate to the two oxygen ligands, allowing the oxygen ligands a greater share of the contracted d orbitals than would be available in an octahedrally coordinated system. The vibrational spectra also indicate that the $p_\pi-d_\pi$ interactions of $OsO_2F_3^+$ are weaker than those of the isoelectronic ReO_2F_3 monomer. The vibrational modes of $OsO_2F_3^+$ involving oxygen are globally shifted to lower values than those of ReO_2F_3, in accord with more contracted d orbitals for cationic Os(VIII) than for neutral Re(VII).

(57) (a) Beattie, I. R.; Livingston, K. M. S.; Ozin, G. A.; Reynolds, D. J. *J. Chem. Soc. A* **1969**, 958. (b) Gillespie, R. J.; Landa, B. *Inorg. Chem.* **1973**, *12*, 1383. (c) Griffiths, E.; Edwards, A. J.; Sunder, W. A.; Falconer, W. E. *J. Fluorine Chem.* **1978**, *11*, 119.

(58) Beattie, I. R.; Crocombe, R. A.; Ogden, J. S. *J. Chem. Soc., Dalton Trans.* **1977**, 1481.

(59) Pausewang, G.; Rudörff, W. *Z. Anorg. Allg. Chem.* **1969**, *364*, 69.

Table 5. Experimental and Calculated Raman Frequencies, Assignments and Mode Descriptions for $OsO_2F_3^+$ and Monomeric ReO_2F_3

	freq (cm^{-1})					
exp[b]	$OsO_2F_3^+$[a]		exp[b]	ReO_2F_3[a]		assignts for $OsO_2F_3^+$ and
$OsO_2F_3^+Sb_nF_{5n+1}^-$[d]	LDFT[c]	NLDFT	ReO_2F_3[e]	LDFT	NLDFT	ReO_2F_3, C_{2v} point symm
996 [65]	1022 (15) {961}	995 (14)	1027 (m) [vs]	1015 (47)	988 (45)	$\nu_1(A_1)$, $\nu_{sym}(MO_2)$
940 [25]	1003 (31) {943}	968 (28)	990 (s) [w]	993 (117)	959 (110)	$\nu_{10}(B_2)$, $\nu_{as}(MO_2)$
	740 (105) {696}	751 (199)	676 (s) [n.o.]	681 (187)	626 (178)	$\nu_7(B_1)$, $\nu_{as}(MF_{2a})$
	745 (35) {700}	766 (28)	702 (s) [s]	699 (64)	657 (61)	$\nu_2(A_1)$, $\nu_{sym}(MF_{2a} + MF_e)$
	677 (11) {636}	684 (7)	621 (w) [m]	620 (25)	565 (20)	$\nu_3(A_1)$, $\nu_{sym}(MF_{2a} - MF_e)$
397 [22]	382 (0.2)	412 (2.9)	369 (n.o.) [m]	376 (1)	359 (1)	$\nu_8(B_1)$, $\delta_{as}(F_eMF_a)$
369 [22]	350 (0.2)	329 (1.0)	358 (i.a.) [m]	338 (1)	339 (2)	$\nu_4(A_1)$, $\delta_{sym}(MO_2$ in plane + $F_eMF_a)$
324 [22]	339 (0)	293 (0)	326 (n.o.) [m]	330 (0)	294 (0)	$\nu_6(A_2)$, MO_2 torsion + MF_{2a} torsion
298 [15]	297 (20)	238 (17)	288 (mw) [vw]	292 (38)	227 (43)	$\nu_9(B_1)$, $\delta_{as}(MO_2$ sym out of plane)
272 [20]	273 (3)	268 (3)	272 (w) [vw]	311 (8)	255 (8)	$\nu_{11}(B_2)$, $\delta_{as}(OMF_e + MF_{2a})$
234 [20]	265 (8)	270 (8)	262 (w) [vw]	274 (10)	248 (14)	$\nu_5(A_1)$, $\delta_{sym}(MO_2$ in plane − $F_eMF_a)$
190 [11]	125 (0)	58 (0)		165 (0)	56 (0)	$\nu_{12}(B_2)$, $\delta_{as}(OMF_e - MF_{2a})$
522 [<1,br]						ν(Os---F---Sb)
733 sh						$Sb_nF_{5n+1}^-$
716 [80]						
701 sh						
666 sh						
660 [100]						
608 [5]						
572 [14]						
350 [31]						
323 [1]						
289 sh						
272 [20]						
248 sh						
219 [15]						
205 [10]						
146 [7]						
134 [7]						
95 sh						

[a] Infrared intensities, in km mol^{-1}, are given in parentheses. [b] Values given in square brackets are Raman intensities. [c] The stretching frequencies, $\nu_1(A_1)$, $\nu_2(A_1)$, $\nu_3(A_1)$, $\nu_7(B_1)$, and $\nu_{10}(B_2)$ were scaled by an empirical factor of 0.94 (values in braces). [d] Data from this study. [e] Data from ref 57. Values given are average values from the infrared and Raman spectra. The assignments are revised assignments based on the calculated values. The symbols in parentheses denote relative intensities (very strong (vs), weak (w), medium (m), very weak (vw), very very weak (vvw), inactive (i.a.), not observed (n.o.), broad (br)).

The Os−F stretching frequencies of $OsO_2F_3^+$ are expected between 600 and 750 cm^{-1} on the basis of those observed for F(*cis*-$OsO_2F_3)_2^+$ and the ReO_2F_3 monomer[58] and theoretical calculations (Table 5); however, they are apparently hidden by the intense bands of the polymeric $Sb_nF_{5n+1}^-$ anions and SbF_5. The F_eOsF_a scissors mode is assigned to a moderately intense band at 397 cm^{-1} and occurs at higher frequency than its counterparts in the spectra of *cis*-OsO_2F_4 (350 cm^{-1})[31] and F(*cis*-$OsO_2F_3)_2^+$ (359/360 cm^{-1}). The symmetric combination of the OsO_2 and F_eOsF_a scissors modes at 369 cm^{-1} is assigned by analogy with its counterpart for *cis*-OsO_2F_4 (344 cm^{-1})[31] and related OOsF bends in the spectrum of the F(*cis*-$OsO_2F_3)_2^+$ cation (343/341 cm^{-1}). The remaining bands cannot be assigned with any confidence owing to the high concentration of SbF_5, but their calculated frequencies are reported in Table 5.

The strong Lewis acid character of the $OsO_2F_3^+$ cation is expected to give rise to fluorine bridge interactions with the anion. A broad, weak band at 522 cm^{-1} is tentatively assigned to the Os---F stretch of the fluorine bridge by comparison with the asymmetric Os---F_b---Os stretch of the F(*cis*-$OsO_2F_3)_2^+$ cation (Table 4). The Sb---F stretch has previously been assigned to a broad, weak band at lower frequencies (445−485 cm^{-1})[51,57b] but cannot be assigned with any confidence here.

Computational Results. (a) The $OsO_2F_3^+$ Cation and ReO_2F_3. The calculated geometric parameters for $OsO_2F_3^+$ and ReO_2F_3 are given in Table 6. There is very little difference in the structural parameters at the local and nonlocal levels with the bond distances slightly shorter at the local level as is usually found. The $OsO_2F_3^+$ cation and the ReO_2F_3 monomer have C_{2v} symmetry at both NLDFT and LDFT levels although significantly more grid points had to be used to obtain C_{2v} structures than is usual. Previous calculations on *cis*-OsO_2F_4[31] showed that the Os−O bond distance is calculated to be too long by 0.02−0.05 Å at the LDFT level. For $OsO_2F_3^+$, the Os−O distance is calculated to be shorter by 0.03 Å than the corresponding distance in *cis*-OsO_2F_4. Thus, it is likely that the Os−O distance in $OsO_2F_3^+$ is about 1.66 Å. Although structural parameters for monomeric ReO_2F_3 are not known, the theoretical bond distances are in good agreement with those reported for ReO_3F (Re−O 1.692(3) Å, Re−F 1.859(8) Å).[60] The charges for $OsO_2F_3^+$ and ReO_2F_3 (Table 7) show that the metal has a charge of about +2.0 e in both molecules. The equatorial and axial fluorines of $OsO_2F_3^+$ have average charges of −0.25 e, and the oxygens, charges of −0.15 e. The charges are more negative in the case of neutral ReO_2F_3, with average values of −0.39 e for the oxygen and −0.40 e for the fluorine

Table 6. Calculated Geometries for $OsO_2F_3^+$ and ReO_2F_3

	$OsO_2F_3^+$ (C_{2v})		ReO_2F_3 (C_{2v})	
bond length/angle	NLDFT	LDFT	NLDFT	LDFT
M−O (Å)	1.707	1.696	1.710	1.705
$M-F_{ax}$ (Å)	1.867	1.848	1.900	1.876
$M-F_{eq}$ (Å)	1.868	1.855	1.913	1.894
O−M−O (deg)	111.0	110.0	109.6	110.5
F_{eq}−M−O (deg)	124.5	125.0	125.2	124.7
F_{ax}−M−F_{ax} (deg)	162.5	160.5	161.5	158.8
F_{eq}−M−F_{ax} (deg)	81.3	80.3	80.7	79.4
O−M−F_{ax} (deg)	94.9	95.6	95.3	96.0

Table 7. Atomic Charges (e) for $OsO_2F_3^+$, ReO_2F_3, and $F(cis\text{-}OsO_2F_3)_2^+$

$OsO_2F_3^+$			ReO_2F_3			$F(cis\text{-}OsO_2F_3)_2^+$		
atom	NLDFT	LDFT	atom	NLDFT	LDFT	atom	NLDFT	LDFT
Os	2.04	2.01	Re	1.99	1.94	Os(1)	1.97	1.93
O	−0.15	−0.15	O	−0.39	−0.39	F(1)	−0.30	−0.30
F_{eq}	−0.26	−0.26	F_{eq}	−0.42	−0.41	F(2)	−0.26	−0.26
F_{ax}	−0.24	−0.23	F_{ax}	−0.40	−0.38	F(2a)	−0.26	−0.27
						O(1)	−0.20	−0.19
						O(2)	−0.16	−0.14
						F(3a)	−0.53	−0.54

atoms. The distribution of the charges on the Os [Re] atom is 0.45 [0.02] e in the valence s orbital and 0.18 [0.16] e in the valence p orbitals. There are 1.89 [2.07] e in the $d_{x^2} + d_{y^2} + d_{z^2}$ orbitals and 3.46 [2.79] e in the $d_{xy} + d_{xz} + d_{yz}$ orbitals. The higher total d orbital population of the Os atom (5.35 e) compared to that of the Re atom (4.76 e) is consistent with the greater electronegativity of Os(VIII). Although the *d*-orbital population is higher in $OsO_2F_3^+$, these orbitals are expected to be more contracted, giving rise to lower frequencies for the metal−oxygen vibrational modes of $OsO_2F_3^+$ compared to those of ReO_2F_3 (see **Raman Spectroscopy and Vibrational Assignments**). The 10 highest occupied molecular orbitals have essentially no d character and reside on the lone pairs of the F and O atoms. The LUMO and NLUMO differ in energy by only 0.23 [0.31] eV and are mostly the metal d_{xz} and d_{yz} orbitals, respectively.

The calculated vibrational frequencies for $OsO_2F_3^+$ and ReO_2F_3 are given in Table 5. The LDFT values are in better agreement with the experimental values. Whereas no scaling factor is applied to the ReO_2F_3 data, it was previously shown that a scaling factor of 0.94 for the stretching modes of *cis*-OsO_2F_4[31] is appropriate at the local level. As in the case of *cis*-OsO_2F_4, this scaling factor is too large for the Os−O symmetrical stretching mode. The vibrational spectrum of monomeric ReO_2F_3 isolated in inert-gas matrices has been studied using infrared and Raman techniques and has established that monomeric ReO_2F_3 has C_{2v} point symmetry.[58] The vibrational frequencies obtained from this previous study are compared with the theoretical values in Table 5. The previous assignments of the $\nu_4(A_1)$, $\nu_5(A_1)$, $\nu_8(B_1)$, and $\nu_{12}(B_2)$ bending and $\nu_6(A_2)$ torsional modes of the ReO_2F_3 monomer differ substantially from those calculated in the present work and have been reassigned.

(b) The $F(cis\text{-}OsO_2F_3)_2^+$ Cation. The calculated geometrical parameters for $F(cis\text{-}OsO_2F_3)_2^+$ are given in Table 8. The local and nonlocal structures differ, with the NLDFT structure having C_s symmetry whereas the LDFT structure is derived from the NLDFT structure by rotating one of the Os units by ca. 45° about the Os−F(3) bridge bond. Other than the change in symmetry, the local and nonlocal structures are quite similar although the differences indicate the nature of the interactions between the Os units and the bridging fluorine. The main difference in the two structures is the local geometry about the bridging fluorine. At the local level, the Os−F(3)−Os bond is almost linear compared to a Os−F(3)−Os angle which deviates by 23° from linearity at the NLDFT level, which is in good agreement with the experimental value. In general, the nonlocal bond distances are longer than the values obtained at the local level except for the Os−F(2A) bond distance, which is shorter by almost 0.02 Å. The Os−F(3) distance is longer by 0.04 Å at the nonlocal level and suggests that this interaction will be smaller and the structure will be more like that of the isolated

(60) Lotspeich, J. F.; Javan, A. *J. Chem. Phys.* **1959**, *31*, 633.

Table 8. Observed and Calculated Geometries of $F(cis\text{-}Os_2F_3)_2^+$

		calcd	
	exp	NLDFT[a]	LDFT[b]
Os(1)−F(2) (Å)	1.813	1.855	1.851
Os(1)−F(2a) (Å)		1.872	1.891
Os(1)−F(1) (Å)	1.821	1.877	1.860
Os(1)−F(3) (Å)	2.086(3)	2.182	2.141
Os(1)−O(1) (Å)	1.750	1.722	1.714
Os(1)−O(2) (Å)	1.676	1.701	1.696
F(1)−Os(1)−F(2a) (deg)	86.6	80.5	83.0 [82.6]
F(1)−Os(1)−O(2) (deg)	98.4	100.4	95.0 [95.7]
F(1)−Os(1)−F(2) (deg)	86.6	82.8	86.0 [85.8]
F(1)−Os(1)−F(3) (deg)	80.2	76.3	76.9 [77.2]
F(1)−Os(1)−O(1) (deg)	160.2	154.0	160.6 [160.5]
F(2a)−Os(1)−O(1) (deg)	90.2	90.6	90.9 [93.4]
F(2a)−Os(1)−O(2) (deg)	99.2	99.0	99.4 [100.4]
F(2a)−Os(1)−F(2) (deg)	161.2	158.1	158.3 [158.1]
F(2a)−Os(1)−F(3) (deg)	91.3	86.1	80.2 [80.1]
F(2)−Os(1)-O(1) (deg)	90.2	98.4	93.3 [91.4]
F(2)−Os(1)−O(2) (deg)	99.2	97.8	100.2 [99.2]
F(2)−Os(1)−F(3) (deg)	91.3	76.3	79.1 [80.1]
O(1)−Os(1)−O(2) (deg)	101.4	105.1	103.6 [103.6]
O(1)−Os(1)−F(3) (deg)	80.4	78.7	84.0 [83.5]
O(2)−Os(1)−F(3) (deg)	169.3	173.6	172.3 [172.9]
Os(1)−F(3)−Os(1a) (deg)	155.2	157.1	178.5

[a] At the NLDFT level, F(2) and (F2a) are not symmetry equivalent; F(2c) and F(2b) are symmetry-related to F(2) and F(2a), respectively. [b] The LDFT geometry is derived from the NLDFT geometry by rotating one of the Os units by about 45° around the Os(1)−F(3) bond, so that F(2), F(2a), F(2c), and (F2b) are all independent. The bond distances to the second Os are the same as to the first Os. Only the angles changed, and are given in brackets.

$OsO_2F_3^+$ cation. Comparison with the experimental structure shows that the Os−O(2) bond length is close to where one would predict it to be (1.674 Å in *cis*-OsO_2F_4[31] and 1.66 Å calculated for $OsO_2F_3^+$), but the Os−O(2), Os−F(1), and Os−F(2) bonds are longer than the experimental values, reflecting the unresolved orientational disorder on these three atoms. Moreover, the trend Os−O(1) < Os−O(2), which is observed experimentally (see **X-ray Crystal Structure**), is confirmed by theory. However, the *trans* influence of the oxygen on the Os−F(1) bond length observed in the crystal structure is only apparent at the NLDFT level (Os−F(1), 1.877 Å > average Os−F(2), 1.864 Å). The calculated distance to the bridging fluorine is found to be longer by 0.06 Å at the local level and by 0.10 Å at the nonlocal level.

The charges for $F(cis\text{-}OsO_2F_3)_2^+$ (Table 7) are as expected from the calculations on $OsO_2F_3^+$. The Os atom still has an average charge of +1.95 e, which is slightly less than in $OsO_2F_3^+$. Both the fluorines and oxygens of each OsO_2F_3 group are predicted to be slightly more negative in $F(cis\text{-}OsO_2F_3)_2^+$ than in $OsO_2F_3^+$. The charge on the bridging fluorine is −0.54 e and suggests that a good model for the structure is a fluoride ion bridging two $OsO_2F_3^+$ cations with the negative charge of the bridging fluoride ion delocalized onto the other electronegative ligands. This is consistent with the simplified valence bond description represented by structures **I**−**III** and with the molecular orbitals. The highest occupied molecular orbitals are predominantly the lone pairs on the bridging fluorine, with some delocalization onto the other F and O ligands. There is no evidence for any strong orbital interaction with the metal in the higher occupied molecular orbitals.

The same scaling factor of 0.94, as described under **Raman Spectroscopy and Vibrational Assignments**, was used for the stretching modes calculated at the local level (Table 4). The scaled LDFT values for the Os−O stretches are in good agreement with the experimental values. The assignments are essentially the same at both levels except for the asymmetric

Os_2F_b stretching mode, which was assigned at the local level. The Os−O_b stretches are higher in frequency than the Os−O_t stretches. The splittings of the asymmetric and symmetric components are small, as the two Os centers are quite far apart. The Os−F stretches in each Os group generally follow the bond length trends. A surprising result was the high frequencies of the modes associated with the bridging fluorine. The value for the asymmetric stretch is calculated to be 649 cm^{-1} at the nonlocal level and 494 cm^{-1} at the local level. The symmetric Os---F_b---Os stretching mode could not be identified from either theory or experiment. The symmetric stretch was found to mix with a variety of modes representing motions of the OsO_2F_3 groups around the bridging fluorine. These modes were found in the region of 150 ± 25 cm^{-1} (Table 5). The bending and stretching frequencies involving F_b suggest that there is a strong interaction between the bridging fluorine and the two $OsO_2F_3^+$ cations. The five lowest energy modes correspond to modes that are predominantly motions of the two $OsO_2F_3^+$ cations with respect to each other, with the torsion about the Os−O axis predicted to be very low in energy, which is consistent with the difference in the local and nonlocal predicted structures.

Conclusions

Osmium dioxotetrafluoride behaves as a fluoro base in anhydrous HF in the presence of strong Lewis acids, forming the dinuclear fluorine-bridged F(*cis*-$OsO_2F_3)_2^+$ cation with SbF_5 and AsF_5 in HF solvent and the $OsO_2F_3^+$ cation in SbF_5 solvent. The $OsO_2F_3^+$ and F(*cis*-$OsO_2F_3)_2^+$ cations are the first examples of cations containing osmium in the +8 oxidation state and, although highly oxidized, the cations do not eliminate O_2 at room temperature. The AsF_6^- and $Sb_2F_{11}^-$ salts of the F(*cis*-$OsO_2F_3)_2^+$ cation are stable in the presence of an excess of fluoro acid in HF solution and in the solid state, whereas the $OsO_2F_3^+$ cation has only been stabilized in SbF_5 solvent. The $OsO_2F_3^+$, F(*cis*-$OsO_2F_3)_2^+$, and F$(ReOF_4)_2^+$ [8] cations are the only metal oxide fluoride cations presently known. The stabilities of both osmium(VIII) cations are likely due to the very favorable *cis* arrangements of the oxygen atoms about the osmium, which allow for maximum π-bonding character in the Os−O bonds. Density functional theory calculations show that the geometries of $OsO_2F_3^+$ (C_{2v}) and F(*cis*-$OsO_2F_3)_2^+$ (C_s) established in solution by ^{19}F NMR spectroscopy and in the solid state by Raman spectroscopy and X-ray crystallography are the energy-minimized structures.

Experimental Section

Apparatus and Materials. All manipulations involving air-sensitive materials were carried out under anhydrous conditions in a nitrogen-filled drybox (Vacuum Atmospheres Model DLX) or, in the case of volatile fluorides, on a vacuum line constructed from 316 stainless steel, nickel, Teflon, and FEP (perfluoroethylene−propylene copolymer). Pressures were measured with the use of an MKS Model PDR-5B power supply and digital readout in conjunction with MKS pressure transducers (0−1000 Torr) which had wetted prepassivated Inconel surfaces. A drybox was used for storage of moisture-sensitive compounds and for transferring nonvolatile and low-volatility fluorine compounds such as SbF_3 and *cis*-OsO_2F_4.

All preparative work involving KrF_2, anhydrous HF and AsF_5 was carried out in 4-mm, $^1/_4$-in., and $^3/_8$-in. o.d. lengths of FEP tubing; in general the tubing was fashioned into either one-armed reactors or two-armed T-reactors. The tubing was heat-sealed at one end and connected through a 45° SAE flare to a Kel-F valve. A typical T-reactor consisted of two $^1/_4$-in.-o.d. FEP tubes, sealed at one end and joined to a Kel-F valve by a Teflon T-connector. All reactors were dried on a Pyrex vacuum line and then transferred to a metal vacuum line where they were passivated with F_2 for several hours, refilled with dry N_2, and placed in the drybox for use.

Starting materials which were purified or prepared by standard literature methods are HF,[61] AsF_5,[4] XeF_2,[4] KrF_2,[62] and *cis*-OsO_2F_4.[31] Antimony pentafluoride that had been purified according to the literature method[63] was also treated with 1000 Torr of F_2 at room temperature in its reaction tube for 12−14 h prior to use in a reaction. Antimony trifluoride (Aldrich) was purified by sublimation in a dry Pyrex glass vessel under static vacuum at 250 °C.

Synthesis of F(*cis*-$OsO_2F_3)_2^+Sb_2F_{11}^-$ and Crystal Growing and Solutions of $OsO_2F_3^+$ in SbF_5. In a glovebag purged with dry N_2, 1.4442 g (6.6645 mmol) of SbF_5 was syringed into a passivated $^1/_4$-in.-o.d. FEP reaction tube and taken into a drybox, frozen in a cold well (−196 °C), and loaded with 0.1790 g (0.6003 mmol) of deep burgundy *cis*-OsO_2F_4. On warming to room temperature, the *cis*-OsO_2F_4 dissolved in SbF_5, giving a deep red-orange solution of $OsO_2F_3^+$ which was considerably lower in viscosity than pure SbF_5. The reaction vessel was attached to a metal vacuum line through a copper U-trap cooled to −196 °C, and excess SbF_5 was removed under dynamic vacuum. After 16 h of pumping, an orange microcrystalline solid was observed in the viscous red-orange solution. Assuming no loss of *cis*-OsO_2F_4, 0.2304 g (1.060 mmol) of SbF_5 remained at this point. Pumping for a further 16 h left an orange crystalline solid wetted with SbF_5 (0.1807 g, 0.833 mmol). The SbF_5-wetted orange solid contained the F(*cis*-$OsO_2F_3)_2^+$ cation on the basis of its Raman spectrum, in which peaks attributable to the cation were identical to those observed for a single crystal of F(*cis*-$OsO_2F_3)_2^+Sb_2F_{11}^-$ and for microcrystalline F(*cis*-$OsO_2F_3)_2^+Sb_2F_{11}^-$.

In a dry-nitrogen-purged glovebag, an additional 0.4707 g (2.172 mmol) of SbF_5 was added to the already SbF_5-rich F(*cis*-$OsO_2F_3)_2^+$ solid to give an OsO_2F_4:SbF_5 molar ratio of 1:5. The solid product dissolved, giving a red-orange solution. The Raman spectrum of this solution was obtained and found to be simpler than that of the F(*cis*-$OsO_2F_3)_2^+$ cation and corresponded to the $OsO_2F_3^+$ cation.

In a second preparation for crystal growth, 31.21 mg (0.1046 mmol) of *cis*-OsO_2F_4 was loaded into one arm of a passivated two-arm reactor consisting of two sealed $^1/_4$-in.-o.d. FEP tubes joined to a Kel-F valve through a $^1/_4$-in. Swagelok Teflon tee in a drybox. The other arm of the reactor was loaded with 18.61 mg (0.1047 mmol) of freshly sublimed SbF_3. The reactor was transferred to a metal vacuum line where ca. 1 mL of HF was condensed onto the SbF_3 at −196 °C. The reactor was warmed to −78 °C and pressurized with 1000 Torr of F_2 and then allowed to warm to room temperature. Rapid F_2 uptake was observed with agitation and was initially accompanied by an increase in the volume of colorless solid. With additional F_2 and further agitation, the volume of undissolved solid decreased, and after 2 h, all solid had dissolved, leaving a colorless solution of SbF_5 in HF. The solution was allowed to stand overnight under 1100 Torr of F_2 to ensure that all SbF_3 had been converted to SbF_5 before pouring the HF/SbF_5 solution onto the *cis*-OsO_2F_4. With agitation, a friable orange solid in an orange solution formed within several minutes, with no trace of *cis*-OsO_2F_4 remaining after 10 min. Crystals of the orange adduct were grown from a supersaturated solution generated from the aforementioned HF solution, by warming both arms of the reactor to 40 °C and decanting the orange solution from the undissolved adduct into the free arm of the reactor. On cooling to room temperature over a 12 h period, rod-shaped, red-orange crystals grew in this arm of the reaction vessel. The supernatant solution was decanted back onto the orange solid, and HF was removed from the reactor under dynamic vacuum while both arms of the reactor were cooled to −10 °C. The FEP reaction tube containing the crystalline product was transferred to a drybox equipped with a microscope, and the crystals were removed by cutting open the FEP tube and examined on a dry glass surface. The crystals were sealed in glass Lindemann capillaries (0.5-mm i.d.) and stored at −10 °C prior to mounting on the diffractometer. A preliminary observation of the sealed crystals under a polarizing microscope revealed both single and twinned crystals. The crystal used in this study had the following dimensions: 0.5 × 0.5 × 0.04 mm. Following X-ray data collection,

(61) Emara, A. A. A.; Schrobilgen, G. J. *Inorg. Chem.* **1992**, *31*, 1323.
(62) Christe, K. O.; Wilson, W. W.; Bougon, R. A. *Inorg. Chem.* **1986**, *25*, 2163.
(63) Gillespie, R. J.; Netzer, A.; Schrobilgen, G. J. *Inorg. Chem.* **1974**, *13*, 1455.

the Raman spectrum of the single crystal used for data collection was obtained and was found to be identical to that of a bulk sample of $F(cis\text{-}OsO_2F_3)_2^+Sb_2F_{11}^-$.

Attempted Preparation of the $OsOF_5^+$ Cation. A passivated reactor consisting of a $^1/_4$-in.-o.d. FEP tube sealed at one end and fitted with a 316 stainless steel valve (Whitey ORM2) was loaded with 138.4 mg (0.4640 mmol) of *cis*-OsO_2F_4 in the drybox. On a metal vacuum line, ca. 140 mg (1.1 mmol) of KrF_2 was condensed onto the *cis*-OsO_2F_4 at −196 °C followed by 4 mL of HF and 1.80 mmol of AsF_5. When warmed just above the melting point of HF, the mixture of KrF_2 and *cis*-OsO_2F_4 was observed as a pink solid in the colorless HF/AsF_5 solution. Warming to −20 °C resulted in gas evolution along with the formation of a pale orange solid. After 30 min, no traces of *cis*-OsO_2F_4 remained. Gas evolution continued for several hours at −20 °C and was accompanied by a gradual darkening of the solid orange product. A portion of the gaseous volatiles had a significant vapor pressure at −196 °C. Removal of this gas by pumping through a glass cold trap produced a yellow discharge on excitation with a Tesla coil, typical of F_2. Warming of the reaction mixture to ca. −150 °C, a temperature still well below the freezing point of HF and AsF_5, resulted in an additional gas pressure attributed to Kr.

When gas evolution had ceased and volatiles had been removed at ca. −150 °C, the reaction mixture was warmed to −70 °C and the Raman spectrum recorded on the orange solid in the pale yellow HF/AsF_5 solution. Bands which could be attributed to the cation were nearly identical in frequency and relative intensity to those observed for $F(cis\text{-}OsO_2F_3)_2^+Sb_2F_{11}^-$. The remaining bands were assigned to AsF_6^- and FEP. No bands attributable to $As_2F_{11}^-$ were observed.

Preparation of NMR Samples. (a) $F(cis\text{-}OsO_2F_3)_2^+AsF_6^-$/HF and $F(cis\text{-}OsO_2F_3)_2^+AsF_6^-/SO_2ClF$. In the drybox, 49.8 mg (0.167 mmol) of *cis*-OsO_2F_4 was loaded into a 4-mm-o.d. FEP NMR tube flare-fitted to a Kel-F valve. On a metal vacuum line, ca. 0.5 mL of HF followed by 1.5 mmol of AsF_5 was condensed onto the *cis*-OsO_2F_4 under static vacuum at −196 °C. The reaction vessel was then closed and allowed to warm to room temperature. On reaching the melting point of the HF/AsF_5 solution, *cis*-OsO_2F_4 began to react to produce an orange solid and a pale yellow solution. After 10 min at room temperature, all *cis*-OsO_2F_4 had reacted, leaving a friable orange solid in a deep orange solution. After 30 min at room temperature the reaction mixture was frozen at −196 °C and the FEP tube heat-sealed under dynamic vacuum. Solid product remaining in the solution was centrifuged into the top of the tube at 30 °C before carrying out the NMR experiment.

The same procedure was followed for the preparation of a sample of $F(cis\text{-}OsO_2F_3)_2^+AsF_6^-$ in SO_2ClF solvent. Anhydrous HF and excess AsF_5 were removed under dynamic vacuum at −78 °C. The sample was cooled to −196 °C without further warming, and SO_2ClF was condensed onto the solid, followed by heat-sealing under dynamic vacuum at −196 °C.

(b) $F(cis\text{-}OsO_2F_3)_2^+Sb_2F_{11}^-$/HF. In the drybox, 22.69 mg (0.0224 mmol) of $F(cis\text{-}OsO_2F_3)_2^+Sb_2F_{11}^+$ was loaded into a 4-mm-o.d. FEP NMR tube flare-fitted to a Kel-F valve. On a metal vacuum line, ca. 0.5 mL of HF was condensed onto the salt under static vacuum at −196 °C. On warming to room temperature, the solid completely dissolved, giving an orange solution. The solution was frozen at −196 °C and the FEP tube heat-sealed under dynamic vacuum.

(c) *cis*-OsO_2F_4 + SbF_5/HF. In a glovebag purged with dry N_2, ca. 0.8 g (4 mmol) of SbF_5 was syringed into a passivated 4-mm-o.d. FEP NMR tube fitted to a Kel-F valve and transferred into the drybox, cooled to −196 °C in a cold well, and loaded with 0.0303 g (0.102 mmol) of *cis*-OsO_2F_4. The tube was transferred to a metal vacuum line, and 0.03 mmol of HF was condensed in under static vacuum at −78 °C. The reactor was cooled to −196 °C and heat-sealed under dynamic vacuum. On warming to room temperature, the *cis*-OsO_2F_4 dissolved to give a red-orange solution significantly lower in viscosity than the *cis*-OsO_2F_4/XeF_2/SbF_5 solution.

(d) *cis*-OsO_2F_4/SbF_5. In a glovebag purged with dry N_2, ca. 1.7 g (7.8 mmol) of SbF_5 was syringed into a passivated 4-mm-o.d. FEP NMR tube fitted to a Kel-F valve and taken into the drybox, cooled to −196 °C in a cold well, and loaded with 0.0284 g (0.0952 mmol) of *cis*-OsO_2F_4. The tube was removed from the drybox, cooled to −196 °C, and heat-sealed under dynamic vacuum. On warming to room temperature, the *cis*-OsO_2F_4 dissolved to give a viscous, yellow-orange solution in SbF_5.

Nuclear Magnetic Resonance Spectroscopy. All ^{19}F NMR spectra were recorded unlocked (field drift <0.1 Hz h^{-1}) on Bruker AC-300 and AM-500 spectrometers equipped with 7.0464- and 11.744-T cryomagnets, respectively, and Aspect 3000 computers. Fluorine-19 spectra were acquired with a 5-mm combination $^1H/^{19}F$ probe operating at 470.600 MHz and on a 5-mm quad (^1H, ^{13}C, ^{31}P, ^{19}F) probe operating at 282.409 MHz. Free induction decays were accumulated in 32K memories with spectral width settings of 50 kHz, yielding acquisition times of 0.328 s. The number of transients accumulated was typically 2000−5000 using pulse widths of 1.0 μs and no relaxation delays. The free induction decays were processed in 64K memories to give data point resolutions of 1.5 Hz/data point; no line broadenings were applied. The ^{19}F spectra were referenced to an external sample of neat $CFCl_3$ at 30 °C. The chemical shift convention used is that a positive (negative) sign signifies a chemical shift to high (low) frequency of the reference compound.

X-ray Structure Determination of $F(cis\text{-}OsO_2F_3)_2^+Sb_2F_{11}^-$. (a) Collection and Reduction of X-ray Data. The crystal of $F(cis\text{-}OsO_2F_3)_2^+Sb_2F_{11}^-$ was centered on a Siemens/Syntex $P2_1$ diffractometer using silver radiation monochromatized with a graphite crystal (λ = 0.560 86 Å). Accurate cell dimensions were determined at −107 °C from a least-squares refinement of the setting angles (χ, ϕ, and 2θ) obtained from 25 accurately centered reflections (with $15° \le 2\theta \le 30°$) chosen from a variety of points in reciprocal space. Integrated diffraction intensities were collected using a $\theta-2\theta$ scan technique with scan rates varying from 3 to 14.65 °/min (in 2θ) and a scan range of ±0.55° so that the weaker reflections were examined most slowly to minimize counting errors. Since a preliminary determination of the unit cell revealed that the system was *I* centered, the data were collected under the *I* system, with $0 \le h \le 20$, $0 \le k \le 21$, and $0 \le l \le 23$ and $3 \le 2\theta \le 60°$. During data collection, the intensities of three standard reflections were monitored every 97 reflections to check for crystal stability and alignment. Over the course of data collection, no decay was observed. A total of 2663 reflections were collected, out of which 93 were standard reflections. A total of 2332 unique reflections remained after averaging of equivalent reflections, of which 1637 satisfied the condition $I \ge 2\sigma(I)$ and were used for structure solution. Corrections were made for Lorentz and polarization effects, while an empirical absorption correction was applied to the data using the ψ-scan method ($\Delta\phi = 10°$; $\mu\bar{R} = 3.464$).

(b) Crystal Data. $F_{18}O_4Os_2Sb_2$ (fw = 1029.9) crystallizes in the orthorhombic space group *Imma*; a = 12.838(3) Å, b = 10.667(2) Å, c = 11.323(2) Å, V = 1550.7(8) Å^3; D_{calc} = 4.411 g cm^{-3} for Z = 4. Ag Kα radiation (λ = 0.560 86 Å, μ(Ag Kα) = 1.999 cm^{-1}) was used.

(c) Solution and Refinement of the Structures. The first model used assumed a 1:1 ratio of *cis*-OsO_2F_4:SbF_5. For close packing of oxygen and fluorine ligands, the volume of the unit cell formally required eight *cis*-OsO_2F_4 and eight SbF_5 molecules per cell. The XPREP program[64] confirmed the original cell and showed the lattice to be orthorhombic *I* centered. The two space groups consistent with the systematic absences were the noncentrosymmetric *Ima*2 and the centrosymmetric *Imma* space groups. The structure was shown to be centrosymmetric by an examination of the *E*-statistics (calculated 0.922, theoretical 0.968), and consequently the structure was solved in the space group *Imma*.

The solution was obtained by the conventional Patterson method which located the special positions of two heavy atoms which were assigned as Os (*m*..) and Sb (.*m*.) atoms. The relatively short Os−Os and Sb−Sb distances indicated that both the cation and anion were likely dimetal bridged species. In addition, four atoms were also located around the Os atom, three on special positions (*m*.. and *mm*2) and one

(64) Sheldrick, G. M. *SHELXTL PLUS*, Release 4.21/V; Siemens Analytical X-Ray Instruments, Inc.: Madison, WI, 1993.

on a general position. The atom located on *mm*2 was the F_b atom. All of these atoms were assigned fluorine scattering factors. The full-matrix least-squares refinement of all these atom positions and isotropic thermal parameters gave a conventional agreement index R ($=\sum||F_o| - |F_c||/\sum|F_o|$) of 0.109. Successive difference Fourier syntheses revealed the remaining fluorine and oxygen atoms and confirmed the presence of the $F(cis\text{-}OsO_2F_3)_2^+$ cation and $Sb_2F_{11}^-$ anion. The location of four general positions for the fluorine *cis* to the F_b atom of the $Sb_2F_{11}^-$ anion implied the existence of a 2-fold disorder which was also resolved for the F_b atom (*.m.*). Consequently, the model used for the $Sb_2F_{11}^-$ anion implied a disorder with the superposition of two anions with identical antimony and fluorine (*trans* to F_b) positions. The site occupancy factors of the disordered fluorine atoms were set equal to 0.5 and 0.25 instead of 1.00 and 0.5, and the U_{eq} of the fluorines *cis* to F_b were set equal. The introduction of these positions (all light atoms being assigned a fluorine scattering factor) and isotropic thermal parameters resulted in a slight drop of the residual factor, R, to 0.089. At this stage, it was possible to distinguish in the osmium environment two bond lengths which were significantly shorter than the other ones, indicating the presence of two Os−O double bonds. Refinement of positional and isotropic temperature parameters for all atoms converged at $R = 0.089$. The introduction of anisotropic thermal parameters for the Os, O, and nondisordered F atoms reduced R to 0.049. At this stage, some of the light atoms around the Os atom revealed a strong anisotropy and exhibited characteristic elongated ellipsoids. This was especially enhanced for the F_b atom (F(3)) and one of the fluorine atoms *cis* to F_b (F(2)). The anisotropy suggested the presence of some positional disorder. The problem was resolved using the updated version of the program SHELXL,[64] which allowed the splitting of the bridging positions, so that the F_b atom was positioned on *.m.* rather than on *mm*2. The positions of the other atoms were too close to be split. The final refinement was obtained by introducing a weighting factor ($w = 1/\sigma^2(F) + 0.006029F^2$) and gave rise to a residual, R, of 0.0469 ($R_w = 0.0500$). In the final difference Fourier map, the maximum and minimum electron densities were +2.68 and −2.65 e Å^{-3}.

All calculations were performed on a 486 personal computer using the SHELXTL PLUS[64] determination package for structure solution and refinement as well as structure determination molecular graphics.

Raman Spectroscopy. Raman samples were excited using the 647.1 nm line of a Kr ion laser (Lexel Laser, Inc., Model 3500), and the spectra were recorded on a Jobin-Yvon Mole S-3000 triple spectrograph system equipped with a 0.32-m prefilter, adjustable 25-mm entrance slit, and a 1.00-m monochromator. Holographic gratings were used for the prefilter (600 grooves mm^{-1}, blazed at 500 nm) and monochromator (1800 grooves mm^{-1}, blazed at 550 nm) stages. The spectrum of the single crystal used for the X-ray structure determination of $F(cis\text{-}OsO_2F_3)_2^+Sb_2F_{11}^-$ was obtained using an Olympus metallurgical microscope (Model BHSM-L-2) to focus the excitation laser to a 1-μm spot on the sample. The spectrum of the $cis\text{-}OsO_2F_4/SbF_5$ solution was recorded at 23 °C in the FEP reaction vessel. The spectrum of solid $F(cis\text{-}OsO_2F_3)_2^+Sb_2F_{11}^-$ was recorded at −110 °C in a sealed 3-mm-o.d. Pyrex tube. Solid $F(cis\text{-}OsO_2F_3)_2^+AsF_6^-$ precipitated from an HF/AsF_5 solution was recorded *in situ* under a layer of liquid HF at −70 °C in the FEP reaction vessel. Solid samples obtained after removal of HF/AsF_5 under vacuum at −78 °C contained traces of $cis\text{-}OsO_2F_4$. Low-temperature samples were cooled in an unsilvered Dewar tube mounted inside the Raman macrochamber by passing a cold stream of N_2 gas, displaced from liquid N_2 with a room-temperature stream of dry N_2 gas, through the tube. Temperatures were measured with a copper/constantan thermocouple gauge (accuracy of ±0.8%). The spectra were recorded by signal averaging with use of a Spectraview-2D CCD detector equipped with a 25-mm chip (1152 × 298 pixels) and at a laser power of 150 mW at the sample and slit settings corresponding to a resolution of 1 cm^{-1}. A total of 15 reads each having 60 s integration times were summed. Spectral line positions were calibrated using the 1018.3 or 730.4 cm^{-1} line of neat indene and are estimated to be accurate to ±1 cm^{-1}.

Computational Methods. All calculations were done with the density functional theory program DGauss[65] on a Cray-C90 computer. The basis set[66] for O and F is of the form (721/51/1) (DZVP2) with a [7/3/3] fitting set. For Os, a norm-conserving[67] pseudopotential[68] (PP) was used, and the valence basis set for Os has the form (4,2/4/3,1) with a fitting basis of the form [7/4/5]. The calculations were done at the local level with the local potential fit of Vosko, Wilk, and Nusair[69] (VWN/PP/DZVP2) and at the nonlocal (gradient-corrected) level with the non-local exchange potential of Becke[70] together with the nonlocal correlation function of Perdew[71] (BP/PP/DZVP2). The geometries were optimized by using analytic gradient methods. Second derivatives were calculated by numerical differentiation of the analytic first derivatives. A two-point method with a finite difference of 0.01 au was used.

Acknowledgment. We thank the donors of the Petroleum Research Fund, administered by the American Chemical Society, for support of this work under ACS-PRF Grant No. 26192-AC3. We also thank the National Science Foundation for the award of a NATO Postdoctoral Fellowship to W.J.C.

Supporting Information Available: Structure determination parameters (Table 9), anisotropic displacement coefficients (Table 10), and equations for the least-squares planes of $F(cis\text{-}OsO_2F_3)_2^+$ (Table 11) and a stereoview ORTEP drawing of the packing in the unit cell of $F(cis\text{-}OsO_2F_3)_2^+Sb_2F_{11}^-$ (Figure 4) (6 pages). Ordering information is given on any current masthead page.

IC951059N

(65) (a) Andzelm, J.; Wimmer, E.; Salahub, D. R. In *The Challenge of d and f Electrons: Theory and Computation*; Salahub, D. R., Zerner, M. C., Eds.; ACS Symposium Series 394; American Chemical Society: Washington, DC, 1989; p 228. (b) Andzelm, J. In *Density Functional Theory in Chemistry*; Labanowski, J., Andzelm, J., Eds.; Springer-Verlag: New York, 1991; p 155. (c) Andzelm, J. W.; Wimmer, E. *J. Chem. Phys.* **1992**, *96*, 1280. DGauss is a density functional program available through the Cray Unichem Project.
(66) Godbout, N.; Salahub, D. R.; Andzelm, J.; Wimmer, E. *Can. J. Chem.* **1992**, *70*, 560.
(67) Troullier, N.; Martins, J. L. *Phys. Rev. B* **1991**, *43*, 1993.
(68) Chen, H.; Kraskowski, M.; Fitzgerald, G. *J. Chem. Phys.* **1993**, *98*, 8710.
(69) Vosko, S. J.; Wilk, L.; Nusair, W. *Can. J. Phys.* **1980**, *58*, 1200.
(70) (a) Becke, A. D. *Phys. Rev. A* **1988**, *38*, 3098. (b) Becke, A. D. In *The Challenge of d and f Electrons: Theory and Computation*; Salahub, D. R., Zerner, M. C., Eds.; ACS Symposium Series 394; American Chemical Society: Washington, DC, 1989; p 166. (c) Becke, A. D. *Int. J. Quantum Chem. Symp.* **1989**, *23*, 599.
(71) Perdew, J. P. *Phys. Rev. B* **1986**, *33*, 8822.